

THIS REPORT HAS BEEN DELIMITED
AND CLEARED FOR PUBLIC RELEASE
UNDER DOD DIRECTIVE 5200.20 AND
NO RESTRICTIONS ARE IMPOSED UPON
ITS USE AND DISCLOSURE.

DISTRIBUTION STATEMENT A

APPROVED FOR PUBLIC RELEASE!
DISTRIBUTION UNLIMITED.

Armed Services Technical Information Agency

Because of our limited supply, you are requested to return this copy WHEN IT HAS SERVED YOUR PURPOSE so that it may be made available to other requesters. Your cooperation will be appreciated.

AD

44732

NOTICE: WHEN GOVERNMENT OR OTHER DRAWINGS, SPECIFICATIONS OR OTHER DATA ARE USED FOR ANY PURPOSE OTHER THAN IN CONNECTION WITH A DEFINITELY RELATED GOVERNMENT PROCUREMENT OPERATION, THE U. S. GOVERNMENT THEREBY INCURS NO RESPONSIBILITY, NOR ANY OBLIGATION WHATSOEVER; AND THE FACT THAT THE GOVERNMENT MAY HAVE FORMULATED, FURNISHED, OR IN ANY WAY SUPPLIED THE SAID DRAWINGS, SPECIFICATIONS, OR OTHER DATA IS NOT TO BE REGARDED BY IMPLICATION OR OTHERWISE AS IN ANY MANNER LICENSING THE HOLDER OR ANY OTHER PERSON OR CORPORATION, OR CONVEYING ANY RIGHTS OR PERMISSION TO MANUFACTURE, USE OR SELL ANY PATENTED INVENTION THAT MAY IN ANY WAY BE RELATED THERETO.

Reproduced by
DOCUMENT SERVICE CENTER
KNOTT BUILDING, DAYTON, 2, OHIO

UNCLASSIFIED

AD No. 444132
ASTIA FILE COPY

THE MUNICIPAL UNIVERSITY OF WICHITA

THE EXPERIMENTAL INVESTIGATION OF A SWEPT-WING
RESEARCH MODEL BOUNDARY LAYER

by Richard E. Wallace

Aerodynamic Report No. 092

for the Office of Naval Research
Contract Nonr-201(C1)

January 1953
University of Wichita
School of Engineering
Wichita, Kansas



THE EXPERIMENTAL INVESTIGATION OF A SWEPT-WING
RESEARCH MODEL BOUNDARY LAYER

by Richard E. Wallace

Aerodynamic Report No. 092

for the Office of Naval Research
Contract Nonr - 201(01)

January 1953
University of Wichita
School of Engineering
Wichita, Kansas

THE EXPERIMENTAL INVESTIGATION OF A SWEPT-WING RESEARCH MODEL BOUNDARY LAYER

SUMMARY

A detailed study of the boundary layer of a semispan, reflection-plane, quarter-scale model of the Douglas F3D-3 swept wing (ONR RM-4) was made as a continuing phase of a program which is to culminate in the application of a boundary layer, circulation control method. Boundary-layer surveys were made at four chordwise and five spanwise points for three attack angles. A few boundary-layer profiles were measured with the inboard flap deflected to 45 degrees. The boundary layer transition was studied by use of the evaporative method, the stethoscope technique and total-head measurements.

Two boundary-layer variables, velocity magnitude and direction, were measured as a function of the normal distance to the wing surface. This produced basic information on the character of the wing boundary layer, its flow direction variations, and its thickness growth along chords parallel to the plane of symmetry and along spanwise constant local-chord percentage lines. This information was translated into displacement and momentum thicknesses parallel and perpendicular to the wing quarter-chord line, and then to the shape parameters for the wing boundary layer. The results showed the boundary-layer parameters, the thickness, and the transition to be functions of the local-chord percentage.

LIST OF FIGURES

- 1.- A sketch of the model and related notations.
- 2.- A sketch of the boundary-layer probe.
- 3.- The complete probe assembly mounted on the swept-wing model.
- 4.- The probe with the shield removed to show the actuating mechanism.
- 5.- Front view of the probe, gantry, and the control arm mounted on the swept-wing model.
- 6.- A rear view of the swept-wing boundary-layer survey apparatus.
- 7.- A transition pattern on the wing as detected by the evaporative method, $\alpha_t = 0^\circ$.
- 8.- Variation of boundary-layer transition point with angle of attack.
- 9.- Transition from total head measurements.
- 10.- Three-dimensional representation of boundary-layer growth in terms of δ/c .
- 11.- Chordwise boundary-layer growth.
- 12.- Spanwise boundary-layer growth.
- 13.- Flow angle variations within the boundary layer.
- 14.- Experimental boundary-layer profiles and flow angles.
- 15.- Chordwise variation of the shape parameter H_x .
- 16.- Spanwise variation of the shape parameter H_y .

INTRODUCTION

The experimental investigation described herein was conducted as a continuation of the research program on the Douglas F3D-3 (ONR RM-4) swept wing. This program, under the sponsorship of the Office of Naval Research, is directed toward procuring fundamental information on the application of a boundary-layer, circulation control system to a swept wing. A preceding report (Ref. 1) showed the experimentally determined lift and pressure distributions, aerodynamic properties, and tuft studies of the wing. In a sense this report is a supplement, since it extends the knowledge in a more detailed fashion to the boundary layer profile, thickness, transition, and flow direction variations.

Several authors (Refs. 2,3,4, and 7) have produced theories and experimental results which demonstrate the behavior of the boundary-layer on an infinite swept wing. However, as noted by Mager (Ref. 5), the work on finite span swept-wing boundary-layer theories (Refs. 5 and 6) has been inadequately substantiated by the sparse experimental data (Ref. 8). While the present data could be used to check such theories, that was considered beyond the scope of this report.

Because the final experiments in this series will be conducted with a hinged leading edge and blowing air over an outboard aileron, the experimental objective was to define the characteristics of the ONR RM-4 swept-wing boundary layer without such a system. It is therefore an attempt to

understand the wing and its surface flow conditions before embarking on a test program complicated by auxiliary innovations such as the aileron, hinged nose and blowing over the aileron.

NOMENCLATURE

α_t = geometric test angle of attack, degrees

δ_f = flap deflection angle, degrees

ψ = flow angle with respect to the symmetry plane, degrees

c = local wing chord measured parallel to the plane of symmetry, feet.

\bar{c} = wing mean aerodynamic chord, feet.

q = local dynamic pressure, $1/2 \rho U^2$, pounds per square foot.

ρ = air mass density (assumed constant), slugs per cubic foot.

p = local static pressure, pounds per square foot.

P_t = total pressure = $p + q$, pounds per square foot.

q_0 = free-stream dynamic pressure = $1/2 \rho \bar{U}_0^2$, pounds per square foot.

\bar{U}_0 = free-stream velocity, feet per second.

x' = curvilinear ordinate measured in a plane perpendicular to the quarter-chord line, feet.

y' = curvilinear ordinate on the wing surface parallel to the quarter-chord line, feet.

z' = curvilinear ordinate normal to and measured from the wing surface, feet.

x = ordinate parallel to the plane of symmetry measured from the leading edge in the chord plane, feet.

y = ordinate perpendicular to and measured from the plane of symmetry in the chord plane, feet.

z = ordinate normal to and measured from the chord plane, feet.

$u_{max} = \sqrt{u^2 + v^2}$ = local maximum velocity in the boundary layer, feet per second.

u = component of the boundary-layer velocity in the x' -direction, feet per second.

v = component of the boundary-layer velocity in the y' -direction, feet per second.

U, V = local potential flow velocity components at the edge of the boundary layer, feet per second.

δ = nominal thickness of the boundary layer

δ_x, δ_y = displacement thickness = $\int_0^\delta (1 - \frac{u}{U}) dz, \int_0^\delta (1 - \frac{v}{V}) dz$

θ_x, θ_y = momentum thickness = $\int_0^\delta \frac{u}{U} (1 - \frac{u}{U}) dz, \int_0^\delta \frac{v}{V} (1 - \frac{v}{V}) dz$

H_x, H_y = shape parameter = $\frac{\delta_x}{\theta_x}, \frac{\delta_y}{\theta_y}$

R = Reynolds number = $\frac{U_0 C}{\nu}$

R_δ = Local Reynolds number based on the boundary layer thickness = $\frac{U_0 \delta}{\nu}$

ν = kinematic viscosity = $\frac{\mu}{\rho}$

CORRECTIONS

No corrections were applied to the data except for the error incurred in the initial probe setting on the surface of the model. It was discovered soon after the tests began that although extreme care was exercised, the first impulse on the actuating mechanism did not always move the nose of the probe off the surface. Experimentally it was verified that the first few points so in error could be corrected by fairing the profiles toward the zero setting and then subtracting the normal distance error indicated by

the difference between the initial point and the faired curve from the profile normal distance ratios. These corrections in most cases were about 2 percent of the total boundary-layer thickness.

Another error which could not be detected from the profile plots was caused by the inverse problem of not having the mouse on the wing surface at the beginning of the movement. Therefore, if the data was initially accurate to ± 2 percent of the thickness, then after the above correction the error in the curves due to the initial setting of the mouse is 0 to ± 2 percent of the boundary-layer thickness with respect to the normal distance ratio z'/c . This also makes the laminar shear stress values obtained from the curves incorrect.

An additional item concerning the flow angle curves close to the surface is worthy of mention. In placing the three tubes on the curved surface the inboard and outboard tubes registered slightly different pressure readings because they were not located at exactly the same distance from the surface and were distorted by surface contact. This problem was particularly aggravated by the steep velocity gradient of the laminar layer. The angular variation curves show the first few points in error by quite large negative angles. An extrapolation of the unaffected angle trend was used in this area since no correction could be made. The velocity profile was not affected because the total-head tube read total pressure for $\psi = \pm 10^\circ$.

APPARATUS

The one-fourth scale model of the Douglas F3D-3 wing was tested in the University of Wichita 7- by 10- foot wind tunnel. A description of the wind tunnel is presented in reference 9. The model (Fig. 1) was constructed of laminated mahogany and finished with sanding sealer and varnish to produce an aerodynamically smooth surface. As in the previous tests (Ref. 1) the plastic button pressure tabs were used to measure the local static pressure. It was found that the static pressures checked very closely with the original pressure distribution tests, so the routine adopted was merely a check procedure when the probe was far enough from the surface for negligible interference.

Figure 2 shows some details and dimensions of the probe. The sensitivity of such a probe and the yaw range for accurate measurements of total pressure are presented in reference 10. Figures 3 through 6 present the mouse, its mechanisms for rotation and normal motion, and the gantry used for the wing mounting. A pneumatically operated cylinder actuated the cog-wheel drive nut of the probe leg. A difficulty with the system was that it moved unidirectionally. Thus, if it became necessary to lower the mouse to check a reading, the operation was halted and the mouse reset manually.

Originally, the mouse unit was designed to rest on small feet extending from a pivot point directly above the

ends of the tube openings. This was discarded for the more rigid gantry structure which probably resulted also in less interference. However, the somewhat bulky mechanism shield and the short leg to the tubes were retained to expedite the investigation.

An inclined manometer at 30 degrees to the horizontal was used to read the total pressure of the nose center tube, to indicate the two outer tube pressures which were kept equal by probe rotation, and to show the tunnel dynamic pressure. A rod extended through the endplate to a position such that an operator could equalize the manometer readings of the angle-sensing tubes and thus obtain the total pressure and the flow angle. A calibration curve provided the correlation between the control rod vernier dial and the flow angle.

Reference 1 provides a detailed description of the wing model. Some of the physical dimensions are shown in figure 1 such as follows:

Wing semispan	= 65.75 in. (Root 9.25 from fuselage)
Root chord	= 36.70 in.
Tip chord	= 13.25 in.
Mean aerodynamic chord	= 26.94 in.
Wing area	= 11.36 ft ²
Aspect ratio	= 5.28
Sweep angle of root - to-tip quarter chord line	= 36°
Root section, NACA 63-011.64	
Tip section, NACA 63-008	

Fuselage & section, NACA 63-012

Flap span = 46 percent wing semispan,

Model scale = one-quarter full scale.

TESTS

The boundary-layer investigation test schedule was:

Wing Sta.	α_t	Local chord positions without flap, $\frac{x}{c} \times 10^2$	Local chord positions with 45° flap, $\frac{x}{c} \times 10^2$
17.75	0°	30, 50, 70	50
	4°	30, 50, 70	50
	8°	30, 50, 70	50
29.06	0°	30, 50, 70	50
	4°	30, 50, 70	50
	8°	30, 50, 70	50
40.41	0°	30, 50, 70, 90	50, 70
	4°	30, 50, 70, 90	50, 70
	8°	30, 50, 70, 90	50, 70
51.75	0°	30, 50, 70, 90	50
	4°	30, 50, 70, 90	50
	8°	30, 50, 70, 90	50
63.10	0°	30, 50, 70, 90	50
	4°	30, 50, 70, 90	50
	8°	30, 50, 70, 90	50

As for the previous tests, the tunnel dynamic pressure was maintained at 26.5 pounds per square foot which corresponded to 103 mph or 39.1 knots. Because of additional screens in the tunnel settling chamber, the turbulence factor reduced to 1.22. Thereby the effective Reynolds number of the wing based on the mean aerodynamic chord became 2.49×10^6 .

DISCUSSION OF THE RESULTS

Initial experiments with the ONR RM-4 swept wing were made to determine the line of transition by three methods which were used with varying degrees of success. The first utilized the evaporative rate differential between laminar and turbulent layers to indicate the transition line from the evaporation of a volatile surface coating (Ref. 11). A turbulent layer has a higher rate of mixing and a greater velocity gradient at the surface than a laminar layer and therefore accelerates surface evaporation. Ethylene glycol (Prestone) was used as the indicating medium to produce the results shown in figure 7. Talcum powder was blown over the wet laminar area after the run to produce the photographic quality contrast. Notice the indication of turbulent wakes behind the clay area and wood screw holes. There seemed to be a reaction between the liquid and the finish or else subsequent experiment surface preparations were not as carefully made because poorer results were produced in the later attempts and the method was abandoned.

A second method involving the acoustical nature of the two boundary-layer types was then used. This method involved a stethoscope attached to the end of a total-head probe which was moved over the model surface in the boundary layer. The line of demarcation between the turbulent and laminar layers as the probe moved forward along the surface was indicated by a reduction in the noise level. Figure 9 shows the results of this investigation. The transition was found to be a function of the local-chord fraction as indicated also by the

evaporative tests. At the most inboard station the observer had the least faith in the results because of the lack of sharpness in the point at which the noise level changed. The probe was particularly difficult to use at station 17.75 near the nose, which may account for the difference in trend of these readings. Most of the point scatter was a function of the curve slope and could therefore be attributed partially to the accuracy in the model angle of attack settings.

Figure 9 shows the results from the third method of transition detection. The survey probe was placed off the surface at a distance where the velocity profiles indicated the maximum velocity difference occurred during the transition from laminar to turbulent boundary-layer flow. Velocity measurements produced a curve of a gradually increasing velocity through the transition zone followed by a decreasing velocity in the turbulent layer. Thus, when the wing attack angle was increased, the velocity was a maximum at the completion of the flow transition from laminar to turbulent (Refs. 12 and 13). This was an inverse approach to moving the probe through the transition zone at a constant angle of attack. A comparison with the stethoscope results showed good correlation.

It was determined that the transition Reynolds number was not constant along the span, but (for $\alpha_t = 0^\circ$ and $\delta_f = 0^\circ$) varied in the following manner:

Station	R_δ , Transition Reynolds No.
17.75	7.48×10^3
29.08	6.08×10^3
40.41	5.17×10^3
51.75	4.21×10^3
63.10	3.09×10^3

This decrease was due primarily to the thinner laminar layer at transition toward the tip and secondarily to the lower velocities over the less thick tip sections. Approximately these same conditions existed for the attack angles of 4 and 8 degrees. As determined from sphere tests the tunnel turbulence factor was 1.22 which corresponds to 0.26 percent turbulence.

A three-dimensional representation of the wing boundary-layer growth for the three attack angles is given by the sketches of figure 10. The growth was affected primarily by the spanwise pressure gradient, the tip vortex strength and, of course, angle of attack. At $\alpha_t = 8^\circ$ the spanwise gradient caused a very pronounced growth outboard along chord percentage lines; this ultimately was the cause of tip flow separation. The influence of the tip vortex on the boundary layer was most prominent at lower lift values, while the increased thickness with angle of attack is seen from successive sketches.

The graphs of figures 11 and 12 present the chordwise and spanwise values of the boundary-layer thickness to an enlarged scale. It was found that the transition points described above were entirely compatible with these curves.

Also, the influence of the trunnion hole clay filler on the transition was in agreement. This turbulent wake was noticed throughout the data and appeared very much wider than shown by figure 7.

In considering the spanwise growth along constant-percentage chord lines it was found that only when plotted as δ/c did the growth appear, but that the actual thickness was virtually constant as shown in the second plot of figure 12. For the forward 70 percent of the wing this was true except where the laminar layer was tripped by the clay area.

Figure 13 is a complete summary of the flow angle variations within the wing boundary layer. These curves do not include the runs with the flap deflected. Negative flow angles (toward the root) were consistently measured at the edge of the layer which was equivalent to the potential flow direction. Then toward the surface the flow was turned by the adverse pressure gradient in the spanwise direction by as much as 15 to 20 degrees at 8 degrees angle of attack.

The aerodynamic force data of reference 1 showed that the boundary-layer information was all obtained on the linear portion of the lift curve. A major increase in flow angle (before separation) occurred between 8 and 9 degrees angle of attack according to the tuft study pictures. This slightly preceded the lift curve break which resulted from reversed flow at the wing tip.

As previously noted, the boundary-layer thickness distribution showed a large interaction at the wing tip between the layer and the trailing vortex. Figure 13 also demonstrates such an interaction, the result tending to decrease the spanwise flow, especially on the surface. The maximum positive flow angle throughout the layer was measured at station 40.41 in each instance.

Figure 14 depicts the experimental boundary-layer profiles and flow angles on the upper surface of the swept wing. The previously discussed transition character of the wing flow is readily seen in these curves. Note that the flow angle axes have been shifted in many instances to maintain all the curves to the same scale.

Several traits of the boundary layer are evident from a comparison of the various curves. In every case the flow variation angle/immediately outside the viscous layer in the potential flow field was found to be zero. This was in contradiction to the two-dimensional swept-wing measurements of reference 7. From reference 1 the uncorrected lift coefficients of the wing at these tested angles of attack were:

$\alpha_t \backslash \delta_f$	0°	45°
0°	0.025	0.755
4°	0.300	1.005
8°	0.570	1.243

Thus a comparison with reference 7 should be valid since the airfoil sections were comparable.

When the flap was deflected to 45 degrees the major change in the boundary-layer profiles was for $\alpha_t = 0^\circ$,

because the transition moved very far forward. However, toward the tip the pressure gradient was steep and the profiles reflected the presence of this strong adverse pressure gradient. From these observations the major influence of the flap was on the tip boundary layer. This was substantiated by the tuft study of reference 1.

The fact that the boundary layer on this wing behaved as a function of the local-chord percentage was predicted by the pressure distributions. Isobars on the upper wing surface were determined as very closely paralleling the local-chord percentage lines except at the tip which was strongly influenced by the vortex flow. A projection of the flow vectors on the isobar field showed clearly the velocity deterioration in a direction normal to the isobars.

Since the nature of the boundary layer showed constancy along the span, the displacement and momentum thickness components were calculated in directions normal and parallel to the quarter-chord line. These values are presented in tables B and C. To complete the analysis corresponding components of the shape parameter, H , were calculated. These H values are shown in figures 15 and 16 as functions of the chord and span. Reference 17 gives the origin and thoughts behind the shape parameter. The consistency of the results reiterated that the boundary-layer characteristics were constant along the local chord percentage lines of the plain wing.

Sta. 17.75		Sta. 29.08		Sta. 40.41		Sta. 51.75		Sta. 62.10	
$\delta_f = 0^\circ$	$\delta_f = 45^\circ$								
.30	0.16	0.13	0.25	0.25	0.98	0.26	0.26	0.26	0.26
.50	0.30	0.64	0.48	0.48	0.98	0.34	0.34	0.56	0.56
= ²	.70	1.04	0.89	0.85	1.37	0.83	1.30	1.30	1.30
= ³	.90			1.45		1.20		1.50	
0.47	.30	0.55	0.59	0.65	1.34	0.77	0.77	0.85	0.85
	.50	0.80	0.91	0.99	1.55	1.65	1.04	1.35	1.35
	.70	1.30	1.45		2.05	2.05	2.05	2.00	2.00
	.90							2.20	2.20
0.68	.30	0.76	0.86	0.99	1.56	1.15	1.15	1.75	1.75
	.50	1.09	1.31	1.40	1.65	----	2.00	2.40	2.40
	.70	1.80	1.85		2.29	----	2.55	2.20	2.20
	.90				3.30	3.30	3.20	3.70	3.70

Table A.- Boundary-layer thickness, $\frac{\delta}{C} \times 10^2$

Note-- the spaces with a dash were investigated but found too erratic to produce acceptable results.

Sta. 17.75		Sta. 29.08		Sta. 40.41		Sta. 51.75		Sta. 63.10	
δ_x/c	δ_y/c								
0 .3c	9.18	9.37	9.61	10.86	12.93	13.54	20.49	19.22	
0 .5c	4.91	4.56	4.18	5.92	10.25	9.76	9.01	8.59	
= a^2	4.07	3.81	4.29	5.97	5.20	7.40	6.52	8.80	
$a^2 = 4c$	"	"	"	6.01	4.93	8.30	8.30	10.14	8.38
0 .3c	3.55	3.06	4.75	4.41	6.50	5.70	6.91	5.31	11.06
0 .5c	4.75	4.17	6.57	6.00	7.45	5.70	5.39	7.32	10.56
= a^2	5.53	4.46	6.76	4.94	8.30	6.33	9.76	8.11	9.79
$a^2 = 9c$	"	"	"	"	8.70	5.82	10.30	8.61	12.32
0 .3c	5.24	3.77	6.08	4.49	7.85	4.49	10.36	6.36	13.03
0 .5c	5.89	3.31	6.69	4.25	8.61	4.35	10.14	6.19	11.13
= a^2	7.09	4.36	7.94	4.63	10.18	5.20	13.38	7.35	13.73
$a^2 = 9c$	"	"	"	"	12.02	5.20	15.08	7.29	14.79

Table B.- Boundary-layer displacement thickness components, $\frac{\delta}{c} \times 10^3$

Sta. 17.75			Sta. 29.08			Sta. 40.41			Sta. 51.75			Sta. 63.10		
θ_x/c	θ_y/c	θ_z/c												
•30	3.48	3.58	3.76	3.61	4.17	4.17	4.60	5.15	7.96	7.25				
•50	2.28	1.98	2.32	2.23	3.14	2.60	4.39	4.17	4.79	4.30				
•70	2.83	2.67	2.89	2.51	4.04	3.50	4.77	4.06	5.77	5.28				
•90					4.17	3.54	5.37	5.37	7.04	5.84				
•40	•30	2.41	2.12	2.93	2.85	4.17	3.77	4.39	3.62	6.83	5.49			
•50	3.29	2.93	4.05	3.84	4.99	4.04	5.26	4.60	6.90	6.41				
•70	3.74	3.12	4.41	3.61	5.52	4.62	6.36	5.59	8.03	6.90				
•90					5.70	4.08	7.18	5.92	8.38	7.92				
•80	•30	3.48	2.64	4.22	3.38	5.11	3.32	5.52	4.44	3.31	4.86			
•50	4.00	2.86	4.29	3.08	5.56	3.14	6.47	4.50	7.32	4.44				
•70	4.33	3.09	4.79	3.27	6.15	2.77	7.78	5.10	8.73	4.15				
•90					6.59	3.81	8.72	5.32	9.01	4.08				

Table C. - Boundary-layer momentum thickness components, $\frac{\theta}{c} \times 10^3$

	Sta. 17.75		Sta. 29.08		Sta. 40.41		Sta. 51.75		Sta. 63.10		
	H _x	H _y									
0	.30	2.64	2.61	2.54	2.57	2.60	2.60	2.90	2.64	2.57	2.65
0.50	.50	2.17	2.29	1.82	1.77	1.90	2.00	2.35	1.89	2.00	2.00
0.70	.70	1.44	1.43	1.49	1.46	1.48	1.50	1.55	1.62	1.68	1.66
0.90	.90					1.45	1.39	1.49	1.49	1.44	1.43
40	.30	1.47	1.44	1.63	1.55	1.56	1.52	1.56	1.60	1.63	1.70
0.50	.50	1.45	1.43	1.62	1.55	1.53	1.41	1.59	1.53	1.54	1.53
0.70	.70	1.47	1.43	1.54	1.38	1.50	1.38	1.54	1.45	1.53	1.50
0.90	.90					1.53	1.43	1.51	1.45	1.51	1.42
80	.30	1.51	1.43	1.44	1.33	1.54	1.35	1.58	1.44	1.57	1.50
0.50	.50	1.47	1.33	1.55	1.38	1.54	1.38	1.57	1.37	1.52	1.39
0.70	.70	1.64	1.41	1.67	1.42	1.66	1.38	1.72	1.45	1.57	1.35
0.90	.90					1.82	1.33	1.74	1.38	1.64	1.38

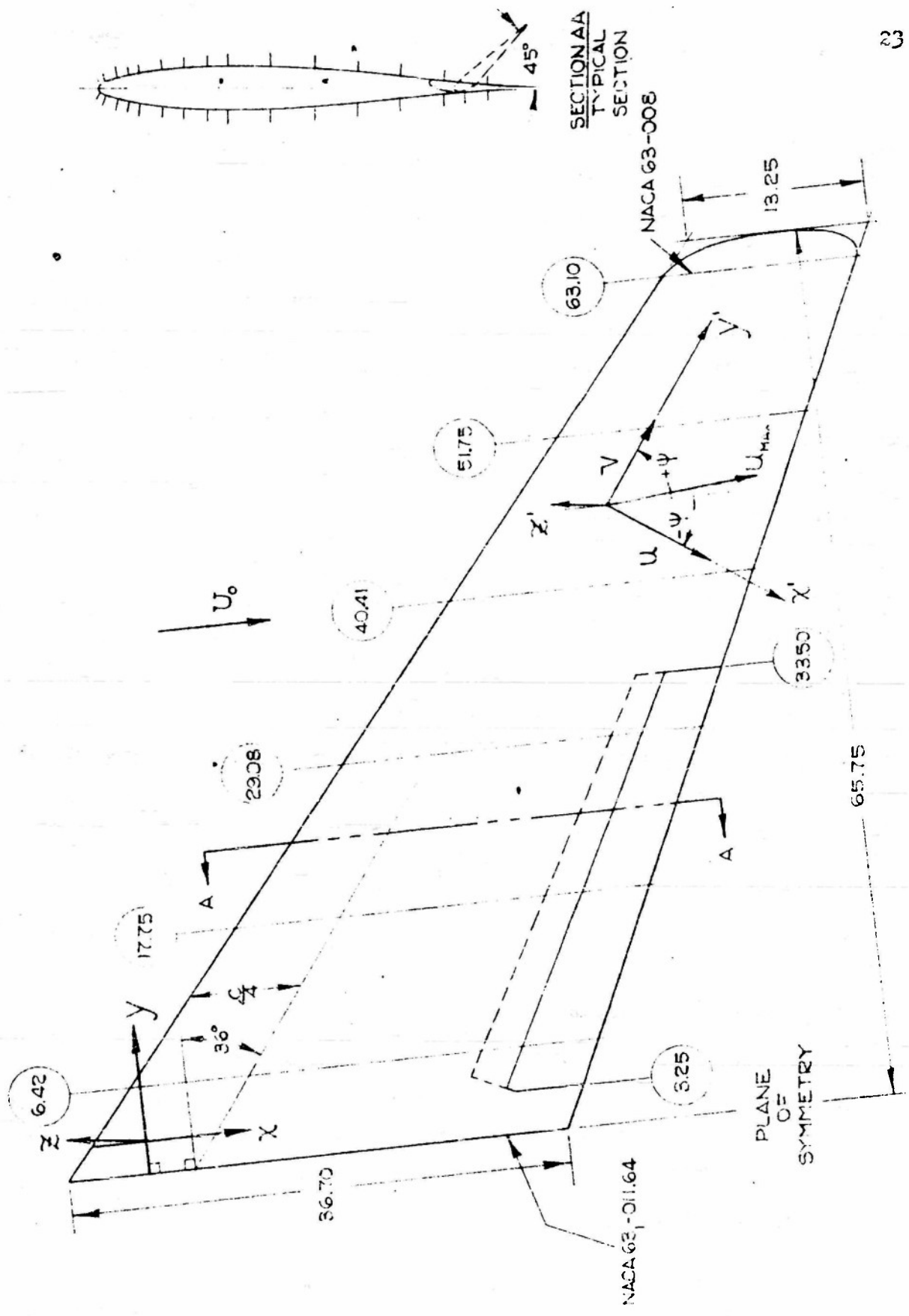
Table D.- Boundary-layer shape parameter components, H

REFERENCES

- 1.- Wallace, Richard E.: Preliminary Report on Wind-tunnel Tests of the ONR Swept-wing Research Model. University of Wichita Aerodynamic Report No. 062, October 1952.
- 2.- Sears, W. R.: The Boundary Layer of Yawed Cylinders. Journal of the Aeronautical Sciences, Vol. 15, No. 1, January 1948.
- 3.- Wild, J. M.: The Boundary Layer of Yawed Infinite Wings. Journal of the Aeronautical Sciences, Vol. 16, No. 1, January 1949.
- 4.- Jones, Robert T.: Effects of Sweep-back on Boundary Layer and Separation. NACA TR 834, 1947.
- 5.- Mager, Artur: Generalization of Boundary-layer Momentum Integral Equations to the Three-dimensional Flows Including Those of Rotating Systems. NACA TR 1067, 1952.
- 6.- Tetervin, Neal: Boundary-layer Momentum Equations for Three-dimensional Flow. NACA TN 1479, October 1947.
- 7.- Altman, John M. and Hayter, Nora-Lee F.: A Comparison of the Turbulent Boundary-layer Growth on an Unswept and a Swept Wing. NACA TN 2500, September 1951.
- 8.- Kueths, A. M.; McKee, P. B. and Curry, W. H.: Measurements in the Boundary Layer of a Yawed Wing. NACA TN 1946, September 1949.
- 9.- Razak, Kenneth: The University of Wichita 7 by 10 Foot Wind Tunnel. University of Wichita Engineering Report No. 022, April 1950.
- 10.- Schulze, W. M.; Ashby, C. J., Jr.; and Erwin, J. R.: Several Combination Probes for Surveying Static and Total Pressure and Flow Direction. NACA TN 2830, November 1952
- 11.- Gray, W. E.: A Simple Visual Method of Recording Boundary-Layer Transition (Liquid Film). RAE TN Aero. 1816, August 1946
- 12.- Silverstein, Abe and Becker, John V.: Determination of Boundary-Layer Transition on Three-Symmetrical Airfoils in the NACA Full-Scale Wind Tunnel NACA TR 637, 1939.
- 13.- Kuethe, A. M. and Schetzer, J. D.: Foundations of Aerodynamics. John Wiley and Sons, Inc., New York, 1950

References (cont'd.)

- 14.- Dryden, Hugh L.: Some Recent Contributions to the Study of Transition and Turbulent Boundary Layers. NACA TN 1168, April 1947.
- 15.- Teterivin, Neal: A Review of Boundary-layer Literature. NACA TN 1384, July 1947.
- 16.- Braslow, A. I. and Visconti, F.: Investigation of Boundary-layer Reynolds Number for Transition on an NACA 65₍₂₁₅₎-114 Airfoil in the Langley Two-dimensional Low-turbulence Tunnel. NACA TN 1704, October 1948.
- 17.- von Doenhoff, A. E. and Teterivin, Neal: Determination of General Relations for the Behavior of Turbulent Boundary Layers. NACA TR 772, 1943.
- 18.- Rubert, K. P. and Persh, J.: A Procedure for Calculating the Development of Turbulent Boundary Layers under the Influence of Adverse Pressure Gradients. NACA TN 2478, September 1951.
- 19.- Page, A.: On Reynolds Numbers of Transition. Aeronautical Research Committee R and M No. 1765.
- 20.- Jacobs, E. N. and von Doenhoff, A. E.: Formulas for use in Boundary-layer Calculations on Low-drag Wings. NACA ACR August 1941, L-319.
- 21.- von Doenhoff, A. E.: Investigation of the Boundary Layer about a Symmetrical Airfoil in a Wind Tunnel of Low Turbulence. NACA ACR August 1940, L-507.
- 22.- Liepmann, H. W.: Investigations on Laminar Boundary-layer Stability and Transition on Curved Boundaries. NACA ACR 3H30, August 1943, W-107.
- 23.- Liepmann, H. W.: Investigation of Boundary-layer Transition on Concave Walls. NACA ACR 4J28, February 1945, W-37.
- 24.- Dryden, Hugh L.: Air Flow in the Boundary Layer Near a Plate. NACA TR 562, 1936.
- 25.- Gault, Donald E.: Boundary-layer and Stalling Characteristics of the NACA 63-009 Airfoil Section. NACA TN 1894, June 1949.
- 26.- McCullough, G. B. and Gault, D. E.: An Experimental Investigation of an NACA 63-012 Airfoil Section with Leading-edge Suction Slots. NACA TN 1683, August 1948.



A sketch of the model and related notations

SCALE: $\frac{1}{10}$ MODEL SCALE

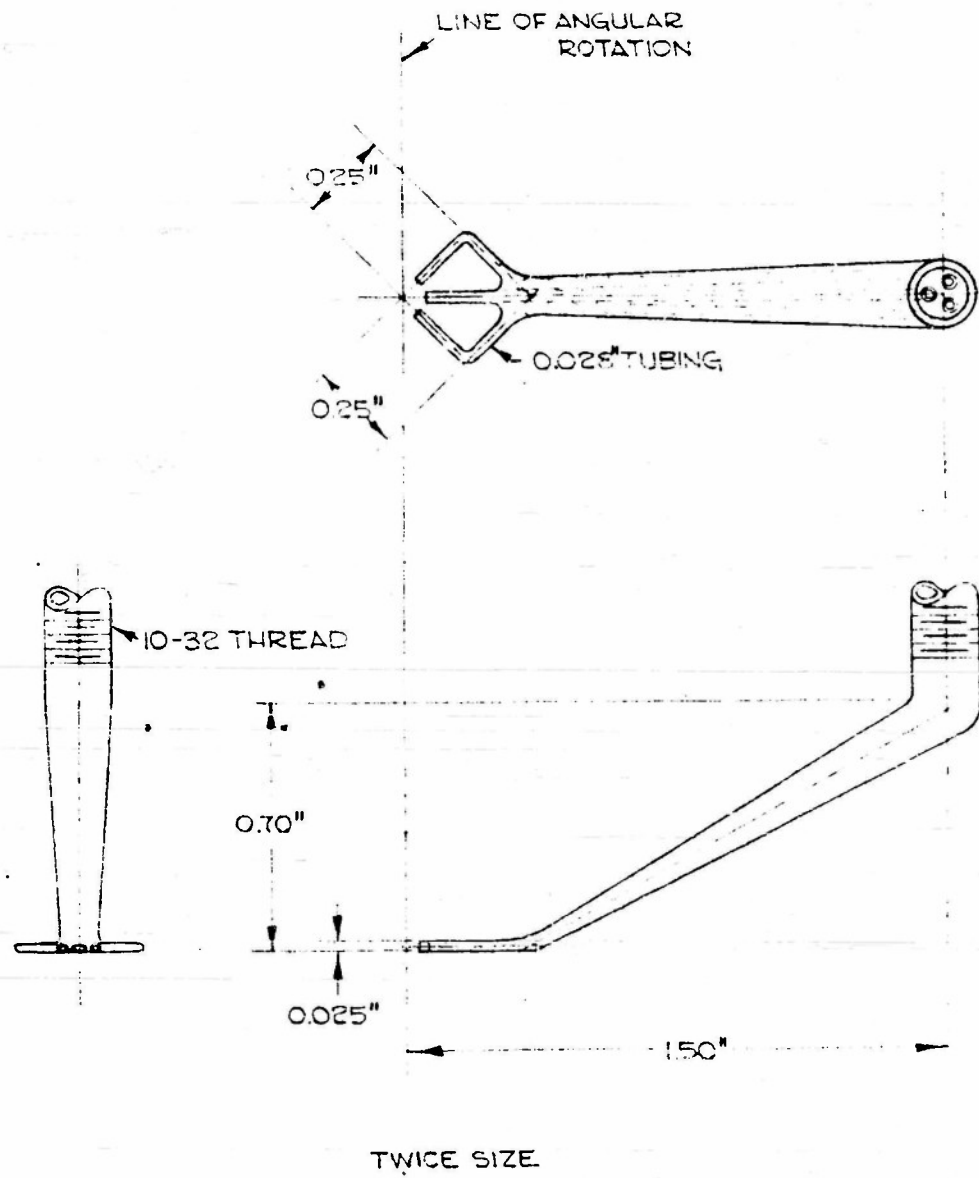


Figure 2.- A sketch of the boundary-layer probe

UNIVERSITY OF WICHITA
SCHOOL OF ENGINEERING
AERODYNAMICS LABORATORY

25

TEST: CNR RR-4
FOR: Office of Naval Research
BY: Richard E. Wallace

TEST NO:
REYNOLDS NO:
DATE: January 1953



Figure 3.- The complete probe assembly mounted on the swept-wing model.

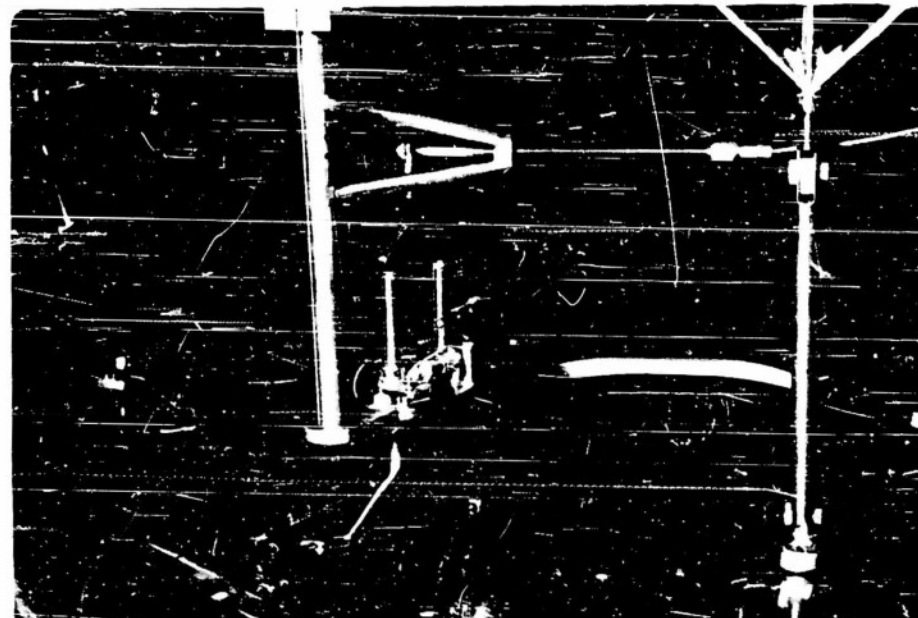


Figure 4.- The probe with the shield removed to show the actuating mechanism.

UNIVERSITY OF WICHITA
SCHOOL OF ENGINEERING
AERODYNAMICS LABORATORY

26

TEST: OMR 84-4
FOR: Office of Naval Research
BY: Richard E. Wallace

TEST NO: _____
REYNOLDS NO: _____
DATE: January 1953



Figure 5.- Front view of the probe, gantry, and the control arm mounted on the swept-wing model.

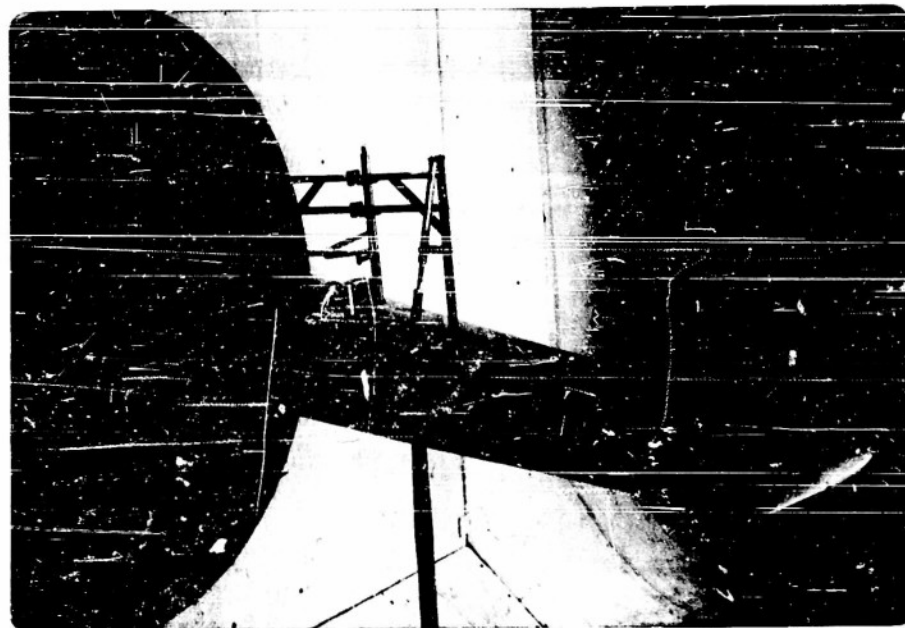


Figure 6.- A rear view of the swept-wing boundary-layer survey apparatus.

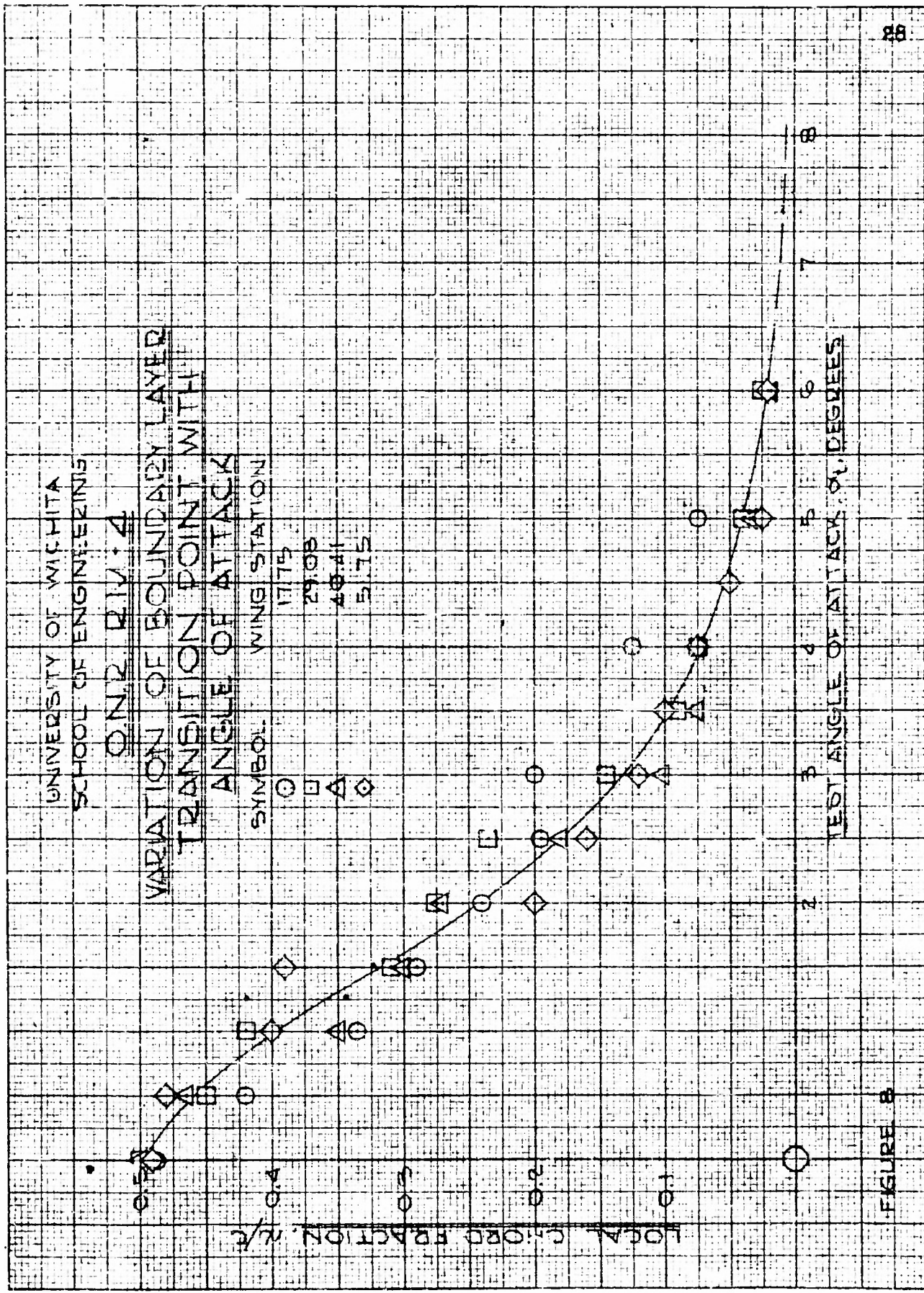
UNIVERSITY OF WICHITA
SCHOOL OF ENGINEERING
AERODYNAMICS LABORATORY

TEST: ONR AF-4
FOR: Office of Naval Research
BY: Richard S. Wallace

TEST NO:
REYNOLDS NO:
DATE: January 1953

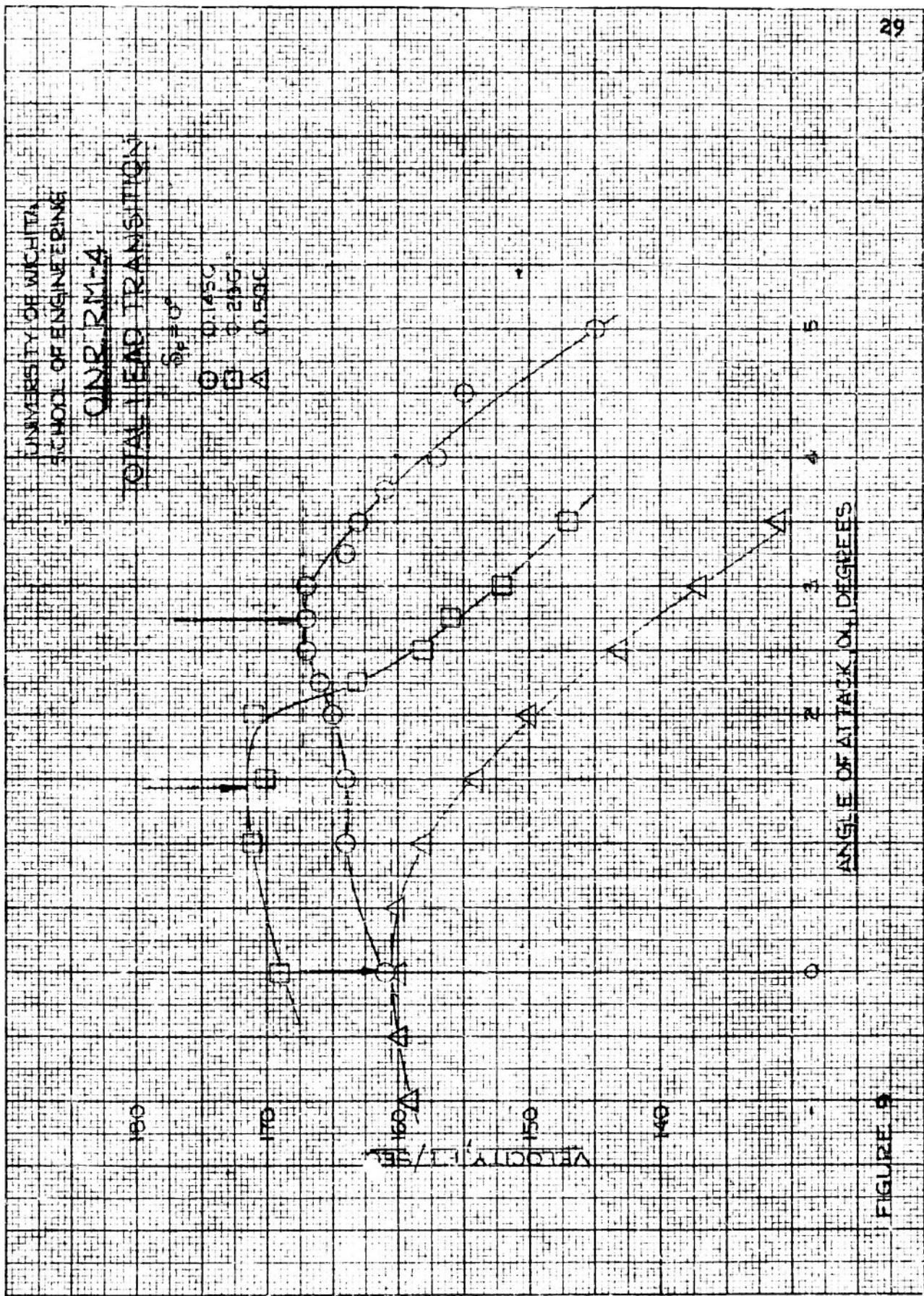


Figure 7.- A transition pattern on the wing as detected by the evaporative method, at $\alpha = 0^\circ$.



ANGLE OF ATTACK ON PELLETS

FIGURE 9



359-11 KUFFEL & ESSER CO.
10 V. 10 to the 1/2 inch, 50 lines per cent.
DIA. 0.5 A

WIND DIRECTION AND VELOCITY IN THE WAKE OF A VARIOUS SIZE CYLINDER

Fig. 3. Effect of cylinder size on wake velocity.

WIND DIRECTION = 0°

WIND VELOCITY = 10 m/sec

WIND VELOCITY = 20 m/sec

WIND VELOCITY = 30 m/sec

WIND VELOCITY = 40 m/sec

WIND VELOCITY = 50 m/sec

WIND VELOCITY = 60 m/sec

WIND VELOCITY = 70 m/sec

WIND VELOCITY = 80 m/sec

WIND VELOCITY = 90 m/sec

WIND VELOCITY = 100 m/sec

WIND VELOCITY = 110 m/sec

WIND VELOCITY = 120 m/sec

WIND VELOCITY = 130 m/sec

WIND VELOCITY = 140 m/sec

WIND VELOCITY = 150 m/sec

WIND VELOCITY = 160 m/sec

WIND VELOCITY = 170 m/sec

WIND VELOCITY = 180 m/sec

WIND VELOCITY = 190 m/sec

WIND VELOCITY = 200 m/sec

WIND VELOCITY = 210 m/sec

WIND VELOCITY = 220 m/sec

WIND VELOCITY = 230 m/sec

WIND VELOCITY = 240 m/sec

WIND VELOCITY = 250 m/sec

WIND VELOCITY = 260 m/sec

WIND VELOCITY = 270 m/sec

WIND VELOCITY = 280 m/sec

WIND VELOCITY = 290 m/sec

WIND VELOCITY = 300 m/sec

WIND VELOCITY = 310 m/sec

WIND VELOCITY = 320 m/sec

WIND VELOCITY = 330 m/sec

WIND VELOCITY = 340 m/sec

WIND VELOCITY = 350 m/sec

WIND VELOCITY = 360 m/sec

WIND VELOCITY = 370 m/sec

WIND VELOCITY = 380 m/sec

WIND VELOCITY = 390 m/sec

WIND VELOCITY = 400 m/sec

WIND VELOCITY = 410 m/sec

WIND VELOCITY = 420 m/sec

WIND VELOCITY = 430 m/sec

WIND VELOCITY = 440 m/sec

WIND VELOCITY = 450 m/sec

WIND VELOCITY = 460 m/sec

WIND VELOCITY = 470 m/sec

WIND VELOCITY = 480 m/sec

WIND VELOCITY = 490 m/sec

WIND VELOCITY = 500 m/sec

WIND VELOCITY = 510 m/sec

WIND VELOCITY = 520 m/sec

WIND VELOCITY = 530 m/sec

WIND VELOCITY = 540 m/sec

WIND VELOCITY = 550 m/sec

WIND VELOCITY = 560 m/sec

WIND VELOCITY = 570 m/sec

WIND VELOCITY = 580 m/sec

WIND VELOCITY = 590 m/sec

WIND VELOCITY = 600 m/sec

WIND VELOCITY = 610 m/sec

WIND VELOCITY = 620 m/sec

WIND VELOCITY = 630 m/sec

WIND VELOCITY = 640 m/sec

WIND VELOCITY = 650 m/sec

WIND VELOCITY = 660 m/sec

WIND VELOCITY = 670 m/sec

WIND VELOCITY = 680 m/sec

WIND VELOCITY = 690 m/sec

WIND VELOCITY = 700 m/sec

WIND VELOCITY = 710 m/sec

WIND VELOCITY = 720 m/sec

WIND VELOCITY = 730 m/sec

WIND VELOCITY = 740 m/sec

WIND VELOCITY = 750 m/sec

WIND VELOCITY = 760 m/sec

WIND VELOCITY = 770 m/sec

WIND VELOCITY = 780 m/sec

WIND VELOCITY = 790 m/sec

WIND VELOCITY = 800 m/sec

WIND VELOCITY = 810 m/sec

WIND VELOCITY = 820 m/sec

WIND VELOCITY = 830 m/sec

WIND VELOCITY = 840 m/sec

WIND VELOCITY = 850 m/sec

WIND VELOCITY = 860 m/sec

WIND VELOCITY = 870 m/sec

WIND VELOCITY = 880 m/sec

WIND VELOCITY = 890 m/sec

WIND VELOCITY = 900 m/sec

WIND VELOCITY = 910 m/sec

WIND VELOCITY = 920 m/sec

WIND VELOCITY = 930 m/sec

WIND VELOCITY = 940 m/sec

WIND VELOCITY = 950 m/sec

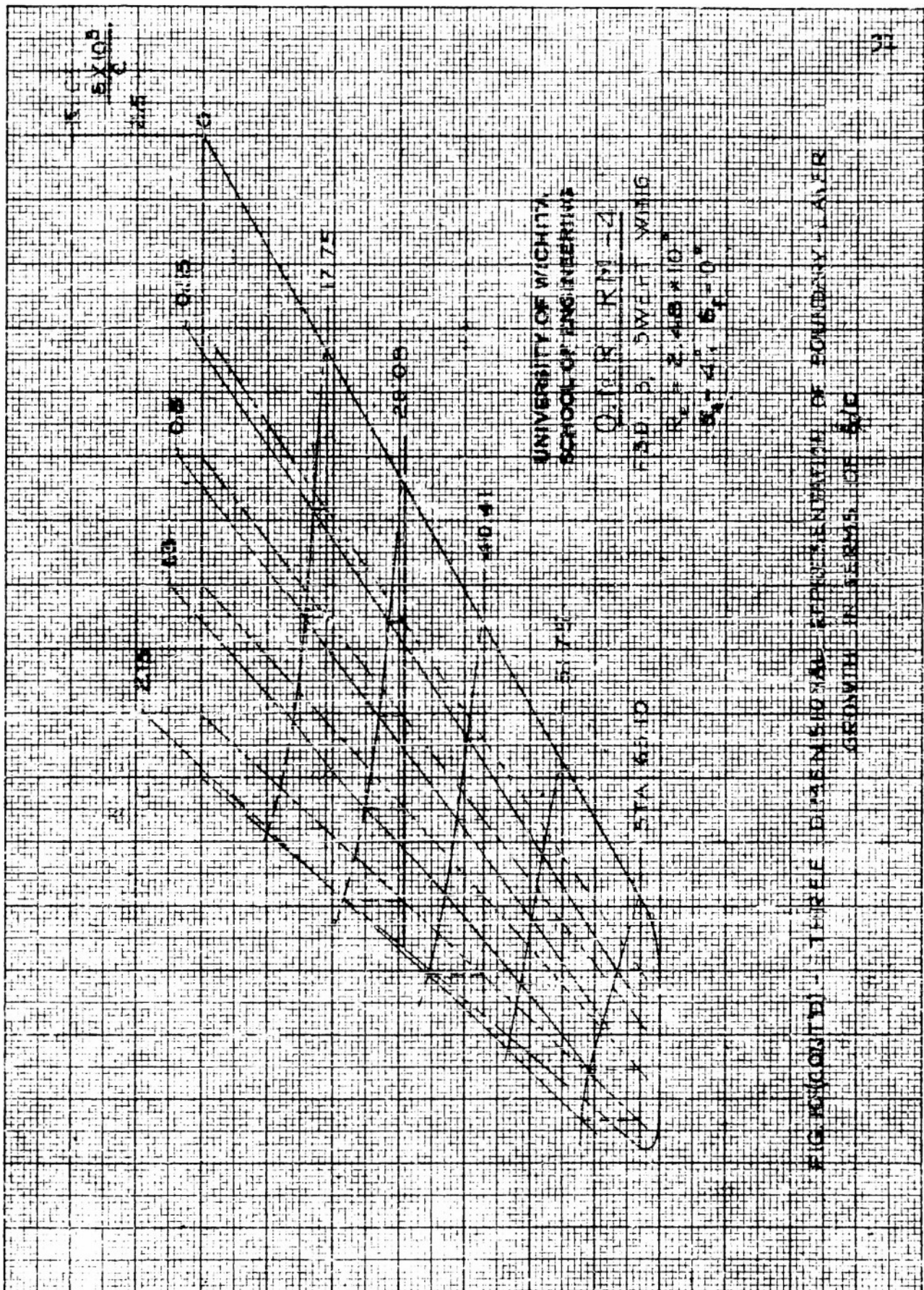
WIND VELOCITY = 960 m/sec

WIND VELOCITY = 970 m/sec

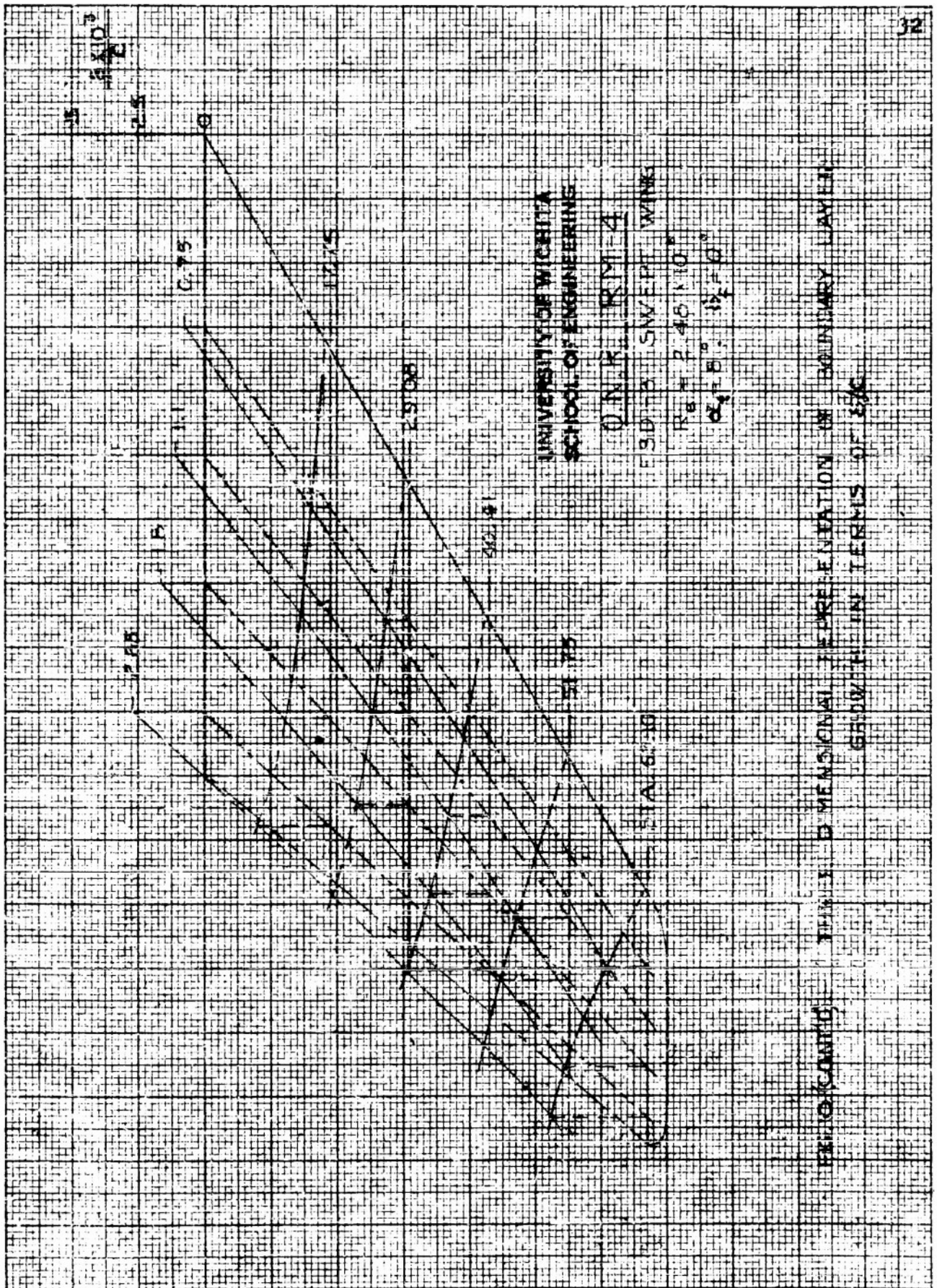
WIND VELOCITY = 980 m/sec

WIND VELOCITY = 990 m/sec

WIND VELOCITY = 1000 m/sec



16 X 16 TO 10 X 10 INCH. PAPER PRINTS ARE MADE.
A
PRINTING CO.

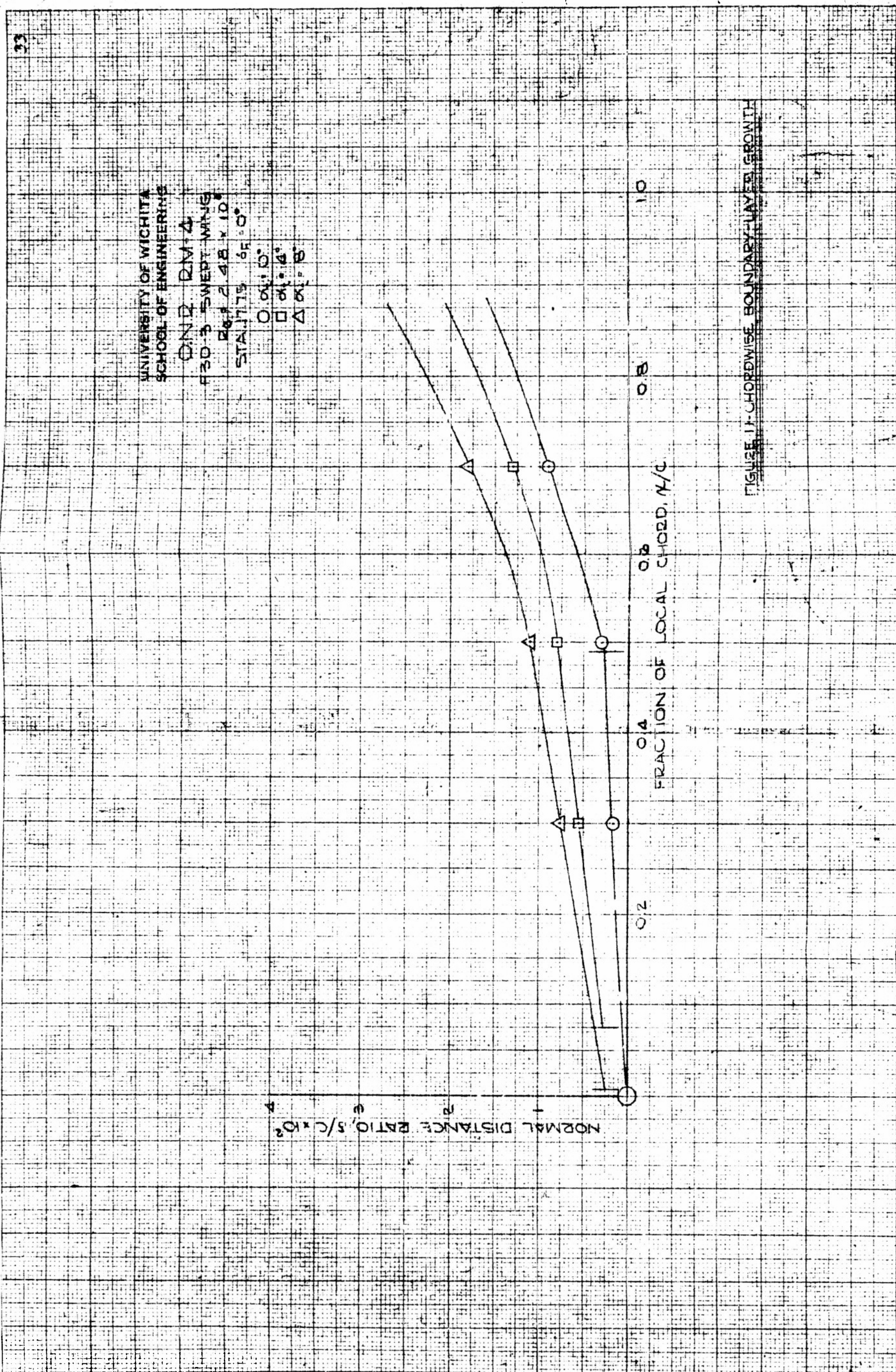


32

THE GENESIS OF THE CONFEDERATION OF STATES OF SOUTH AFRICA

三

10 X 10 Gage. 10 micr. gap. 100% vacuum.
3-26-11 KENNER & ROBERTS CO.



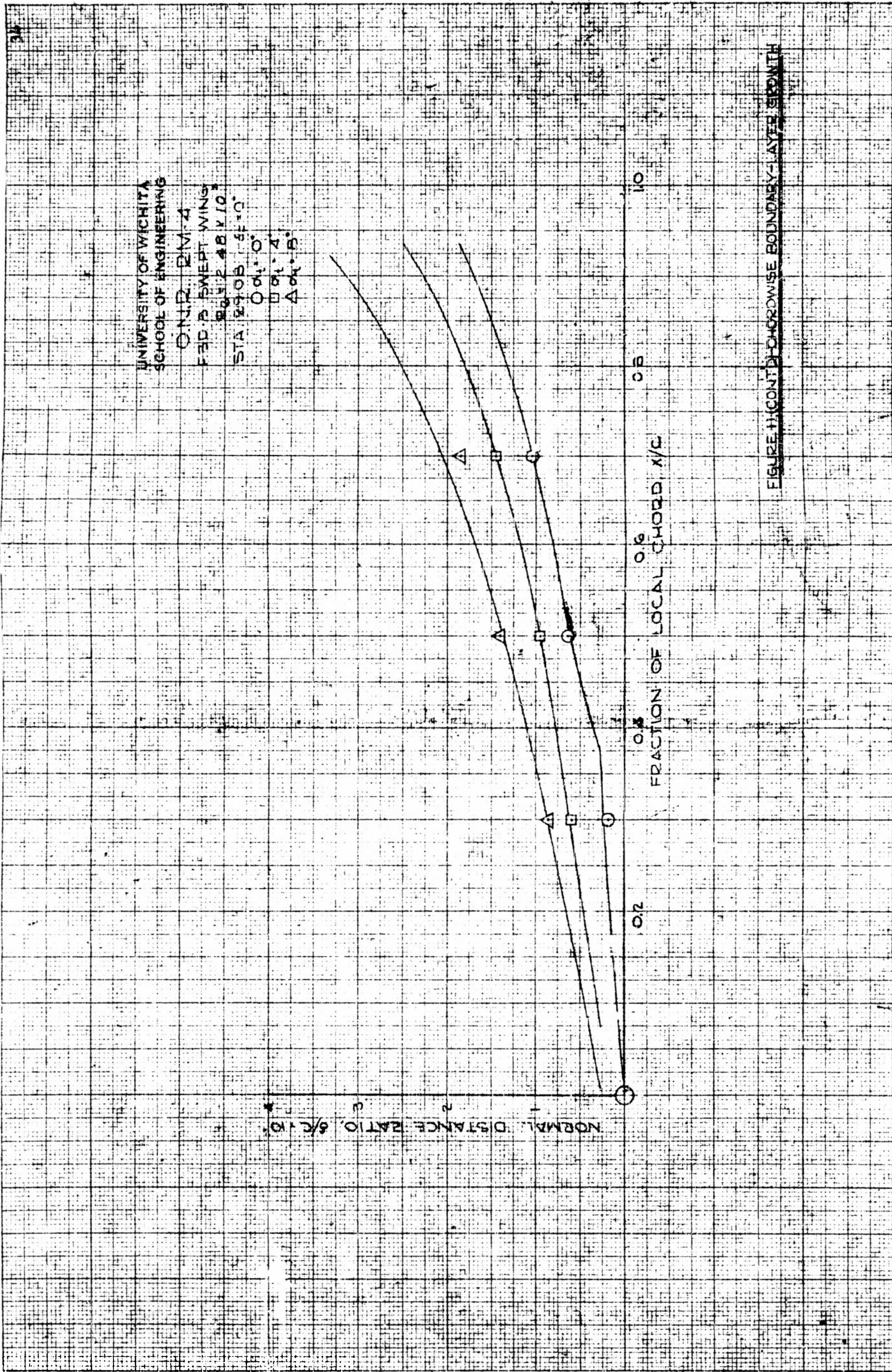


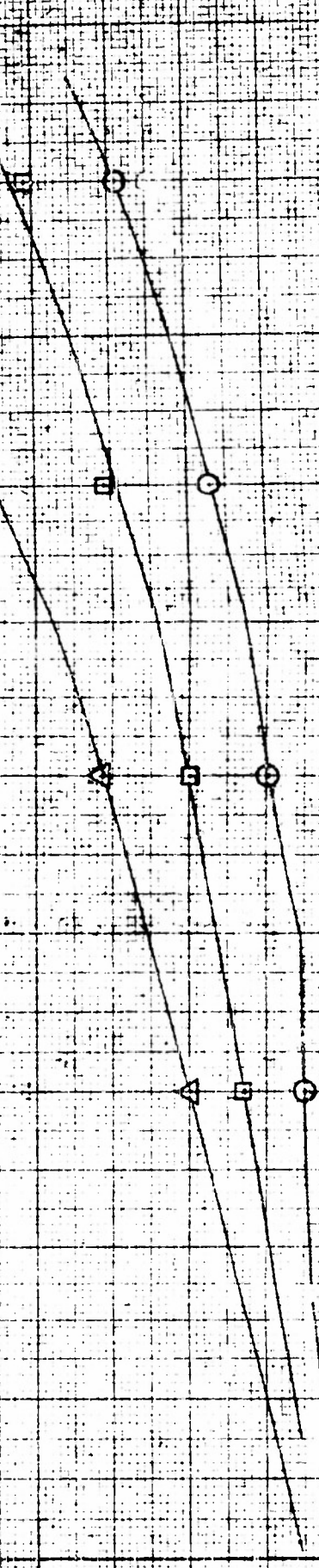
FIGURE 11 CONTOUR CHORDWISE BOUNDARY - LAYER PROFILE

FIGURE 11. COUNTER-CLOCKWISE BOUNDARY

NORMAL DISTANCE DATA 9/11/65

POSITION OF LOCAL CHORD A/C

10
08
06
04
02
00



STA 004-05-0
FID 500-245-100
ONE DIA 4

UNIVERSITY OF MICHIGAN
SCHOOL OF ENGINEERING

UNIVERSITY OF WISCONSIN
SCHOOL OF ENGINEERING

CONFIDENTIAL

CD = 2.5 INCHES

D_c = 2.43 INCHES

STA = 15.300

Oct. 5, 1955

At. S.

NORMAL BRIDGE RATIO, $\sigma/C = 1.0$

FRACTION OF LOCAL CHORD, x/c

0.0

0.2

0.4

0.6

0.8

1.0

FIGURE II (CONT'D) CHORDWISE BURIED LAYER GROWTH

UNIVERSITY OF WICHITA
SCHOOL OF ENGINEERING

ONE 217-4
F3D-3 SWEDT WING
 $2\theta = 24.6 \times 10^6$
STA 2310 SP: 0

TANSON - DETACHMENT RATE: 8/340°

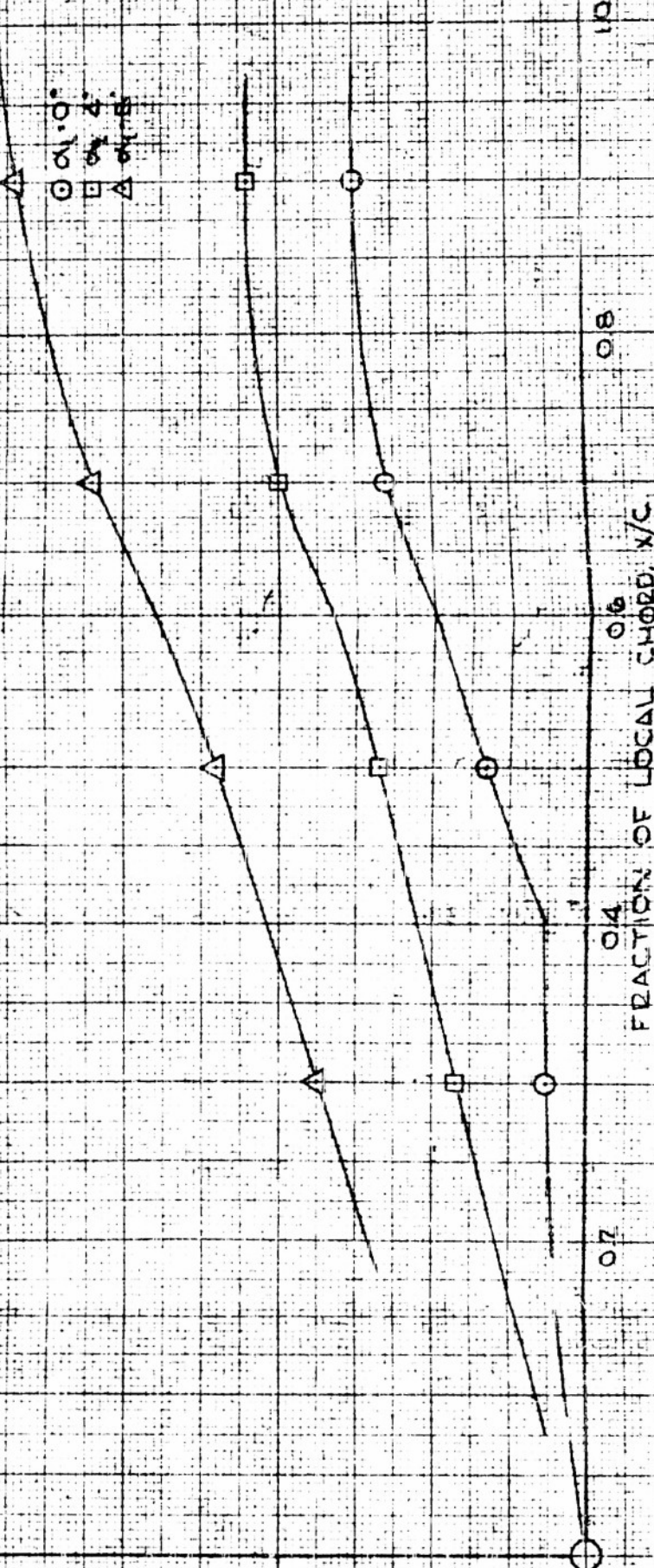
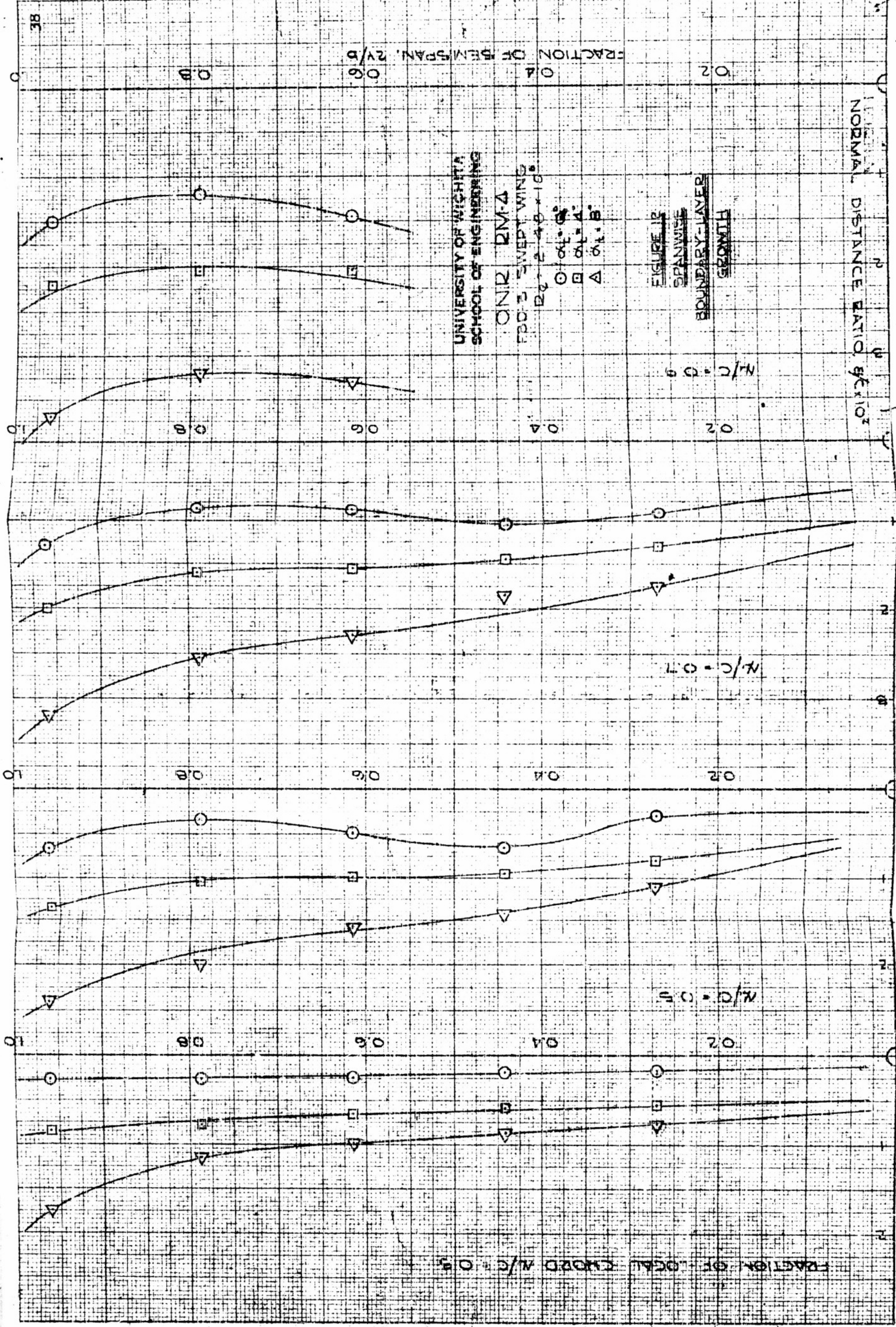
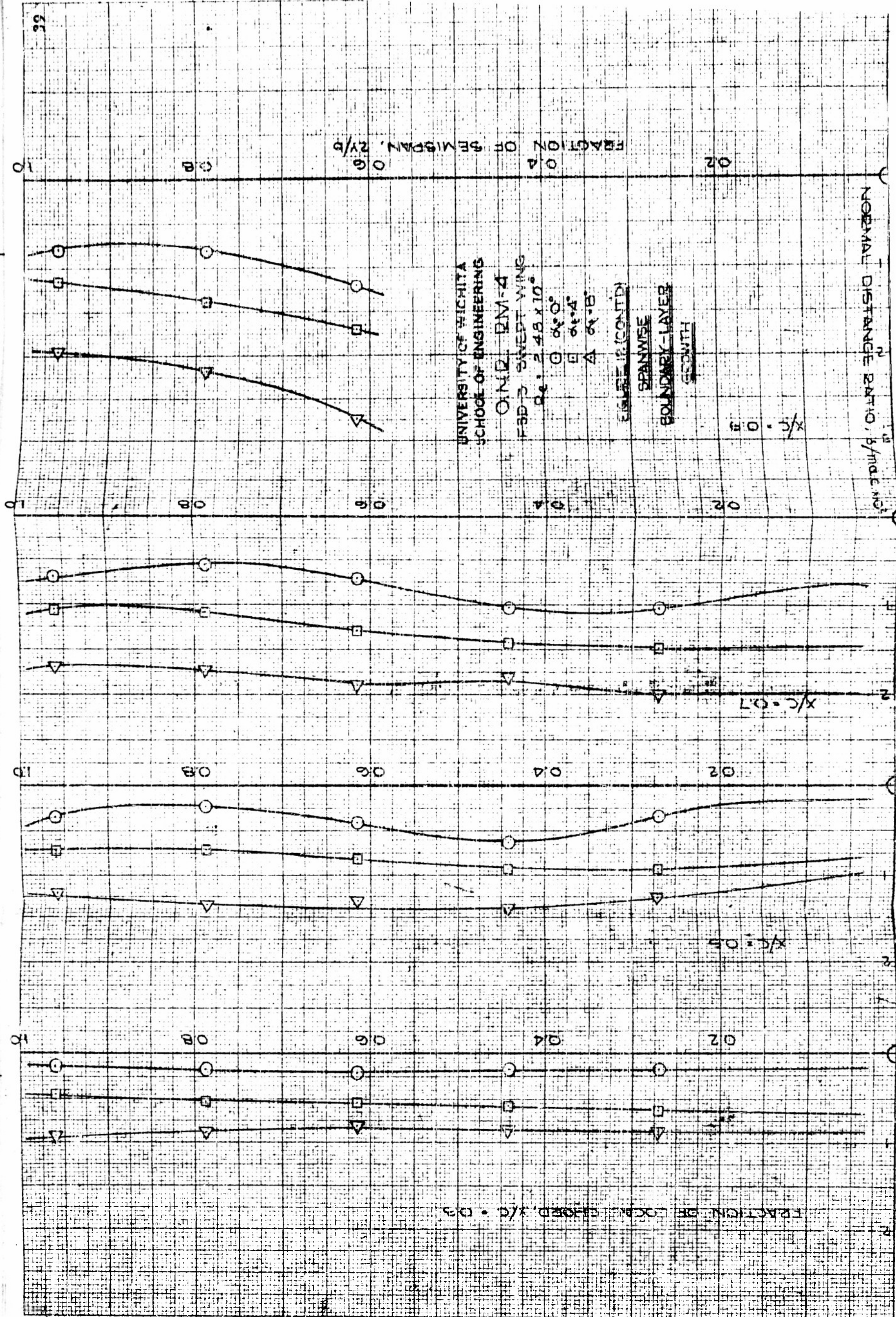
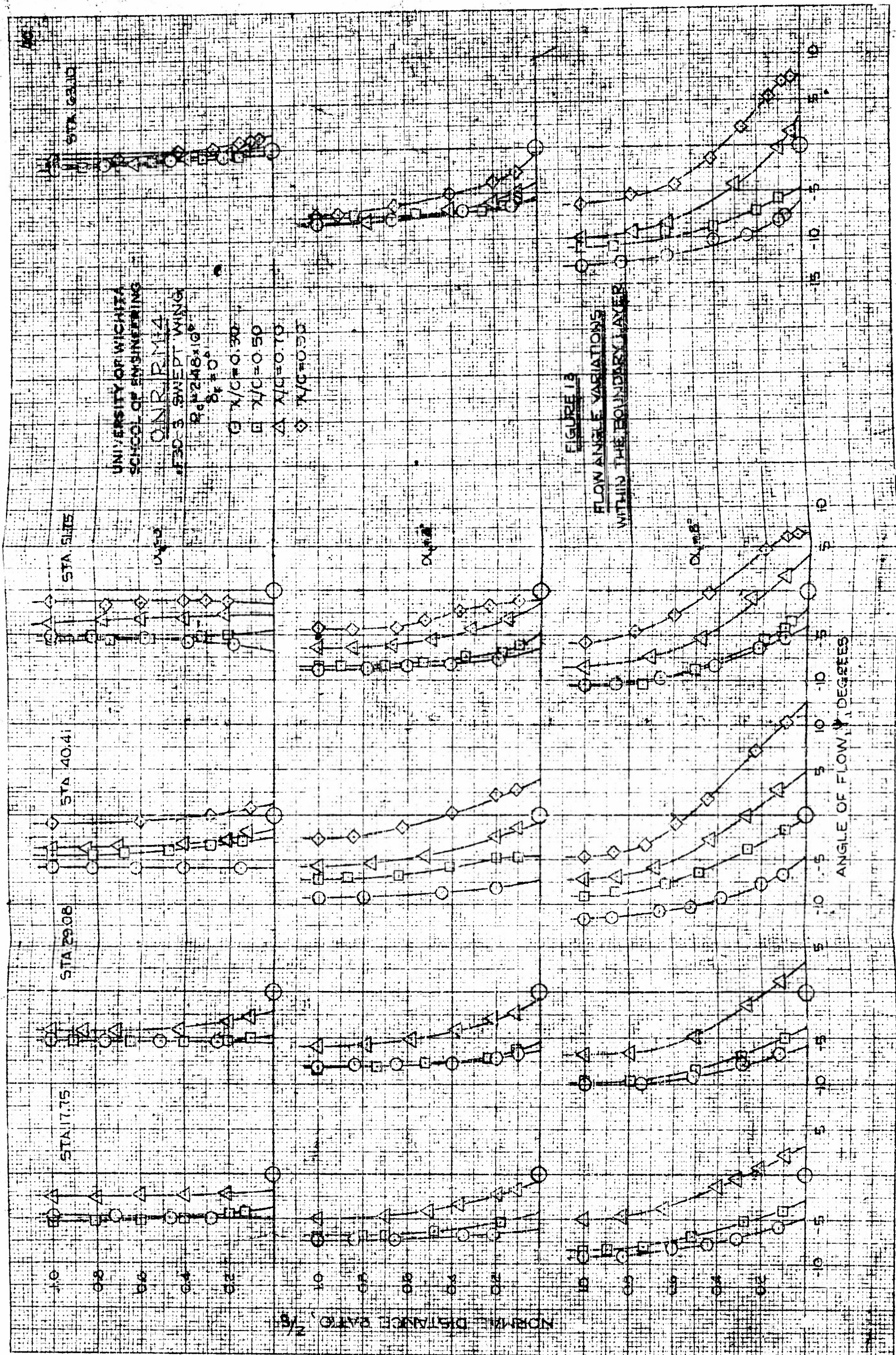
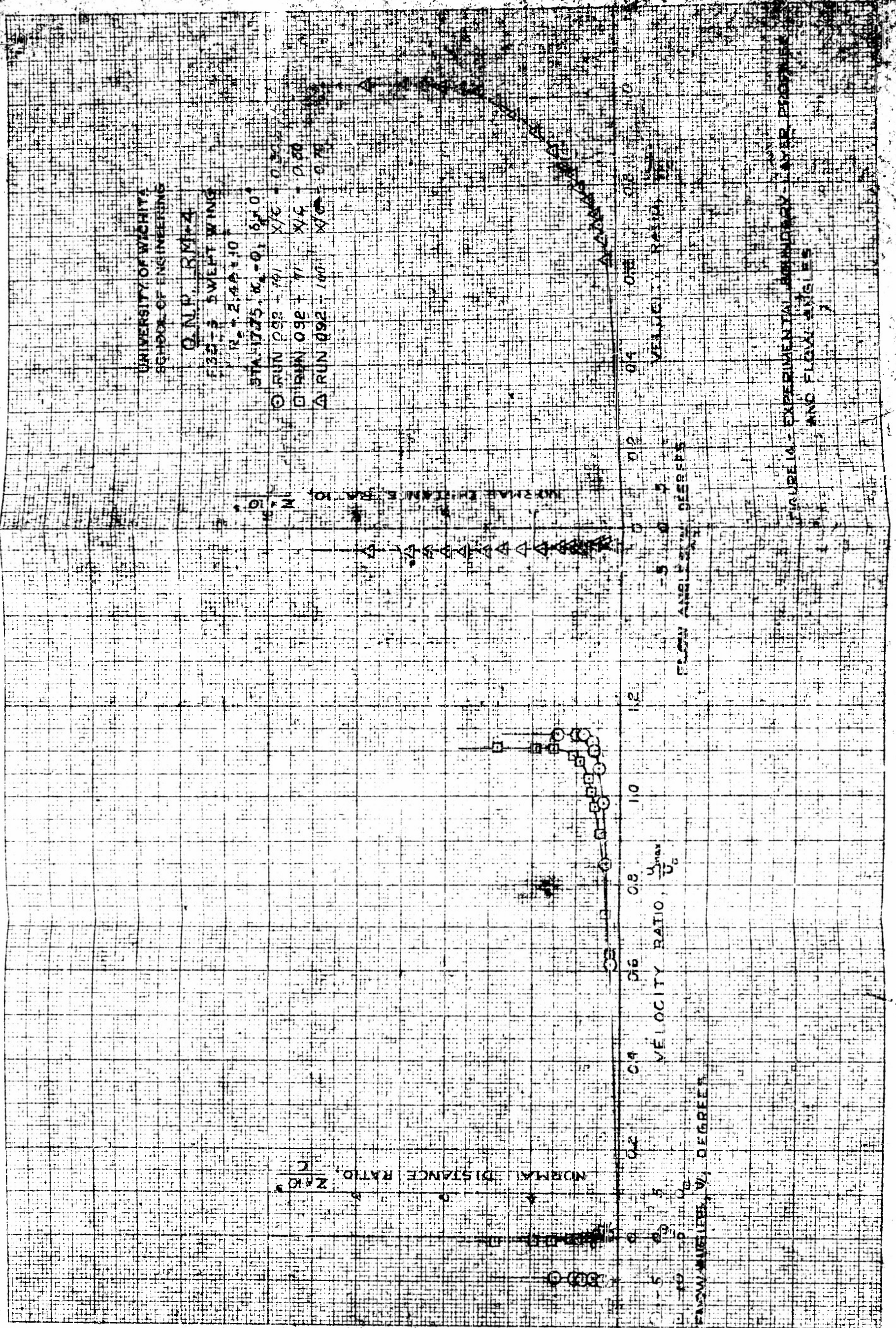


FIGURE 11 (CONT'D)-CHORDWISE BOUNDARY-LAYER GROWTH









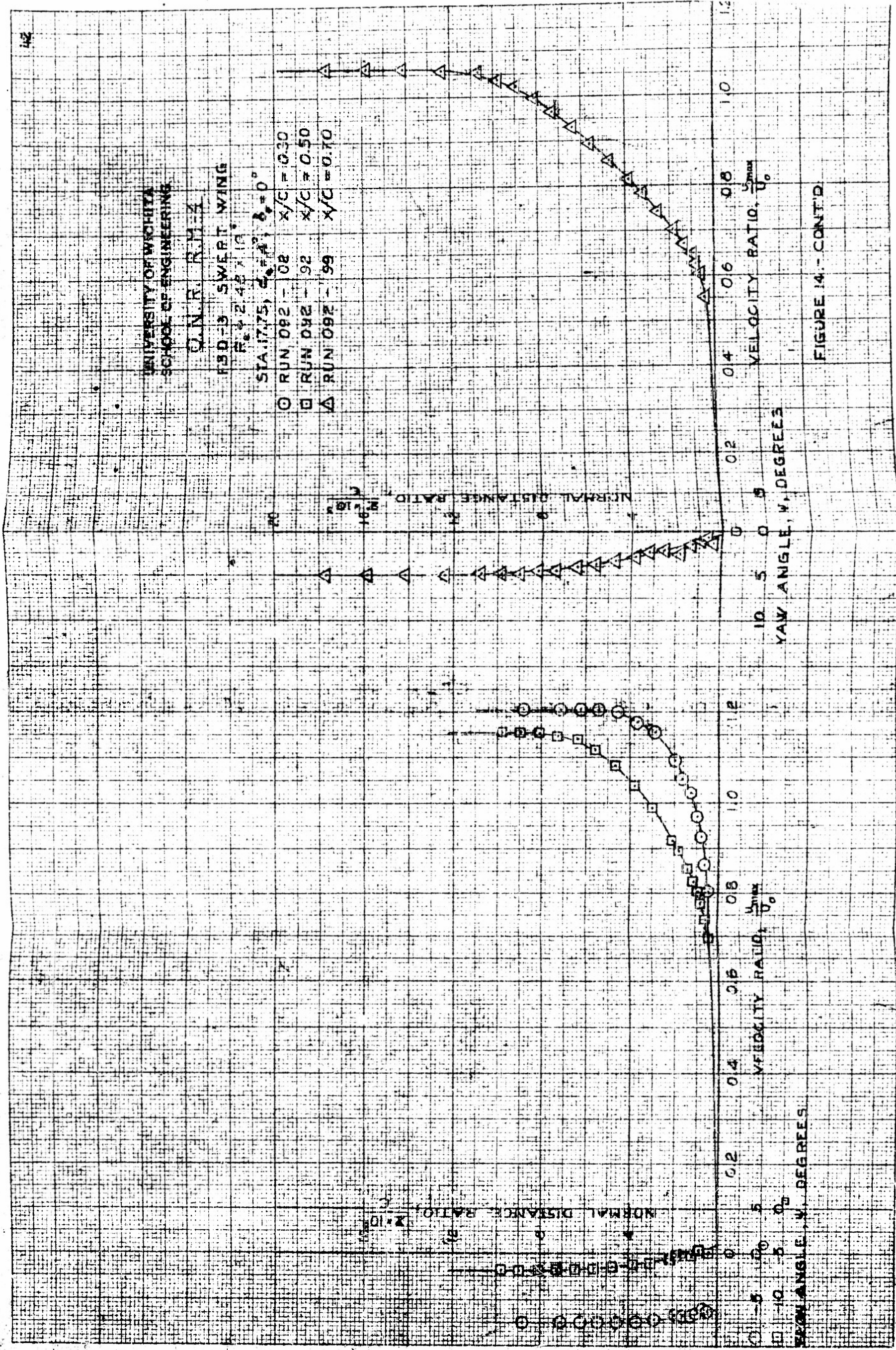
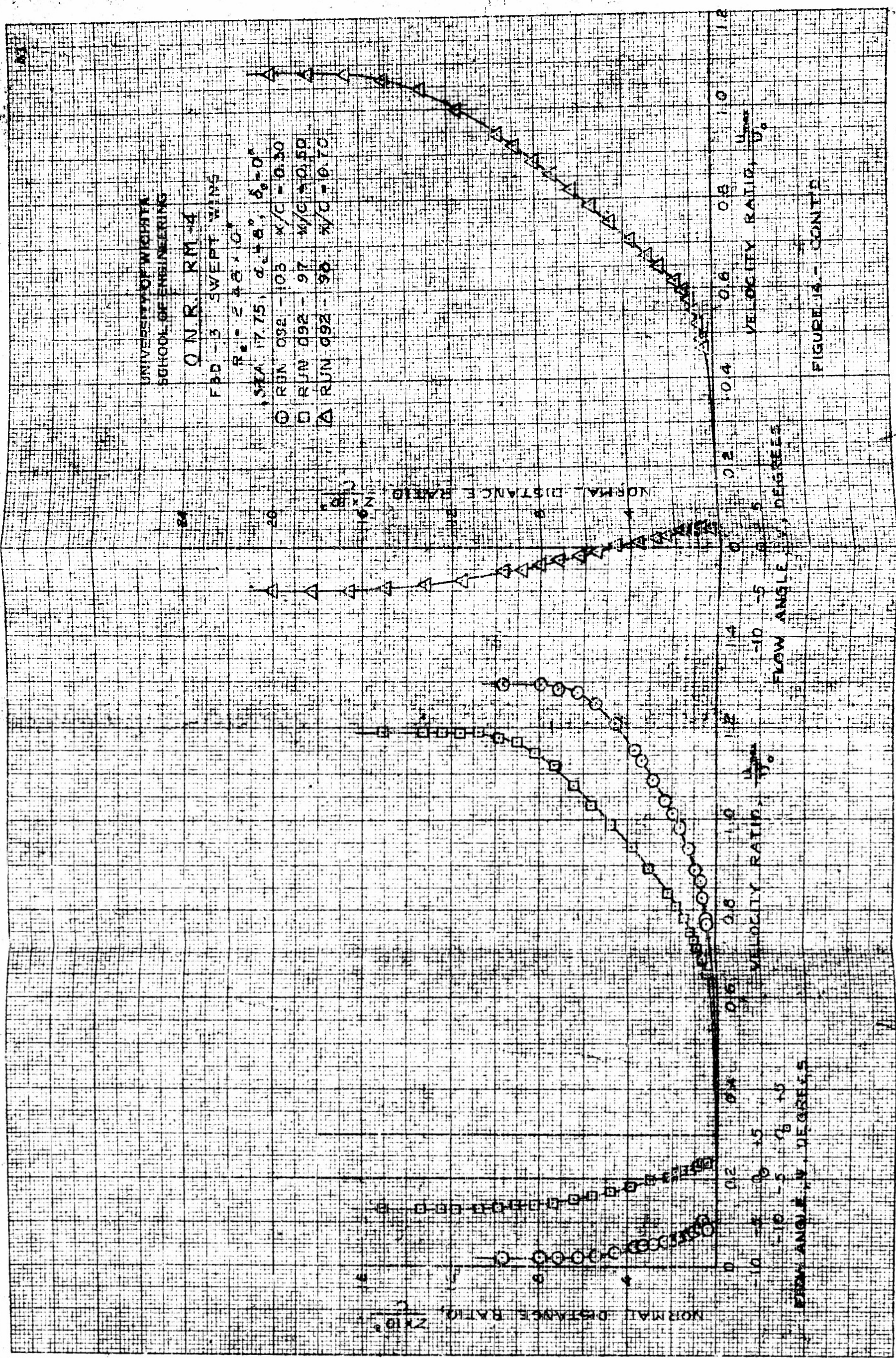


FIGURE 18 - CONT'D.



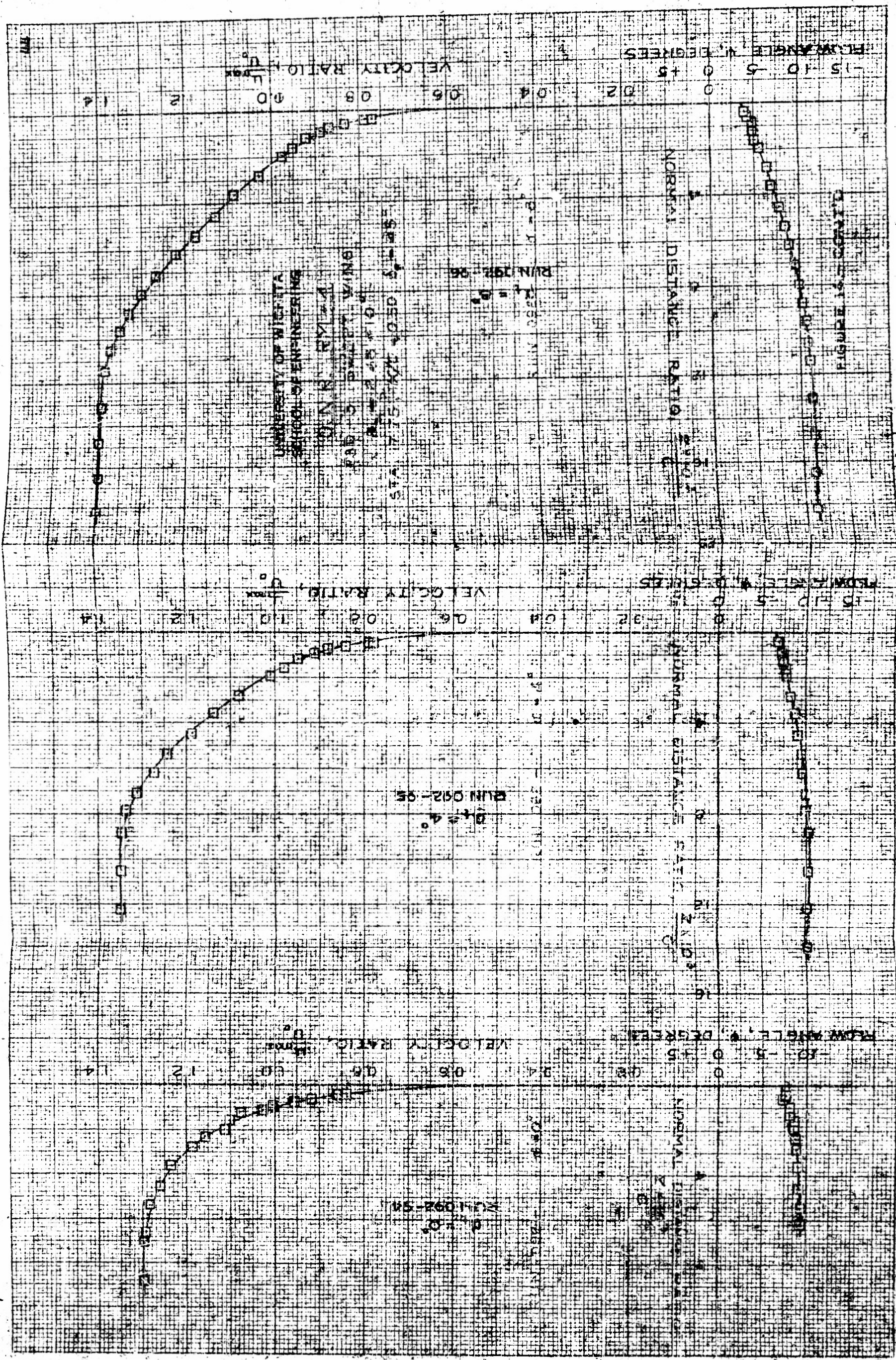
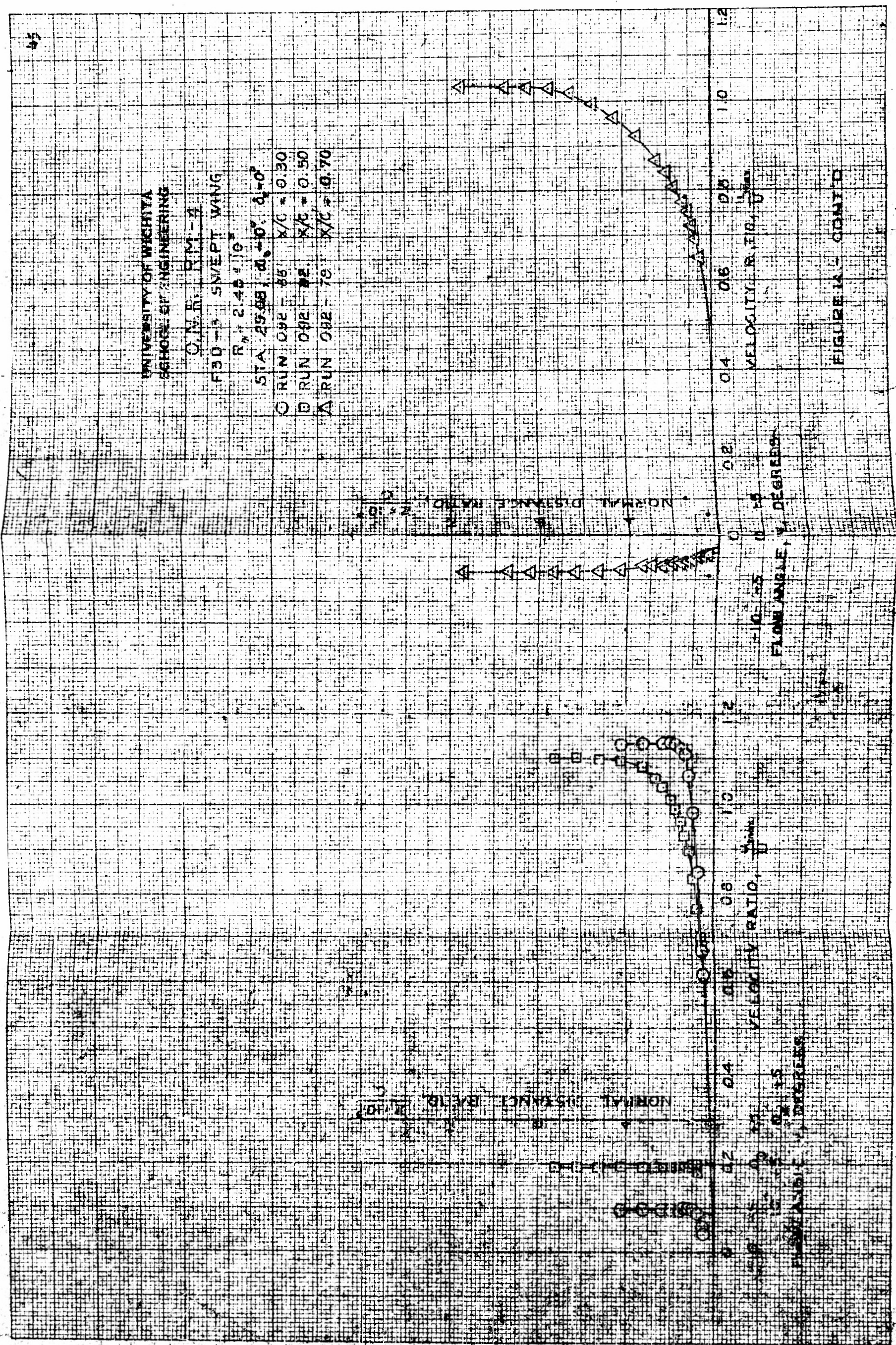
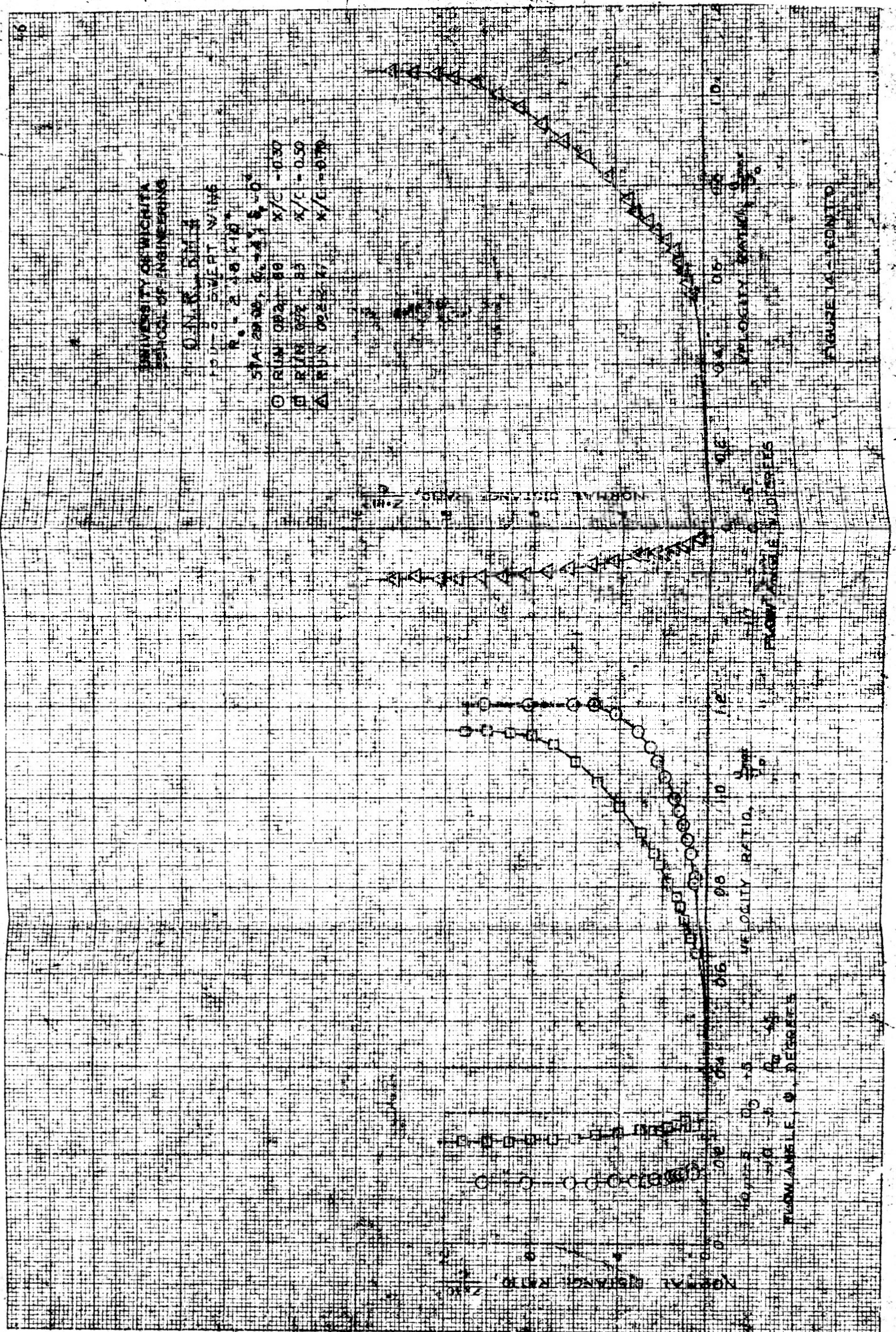
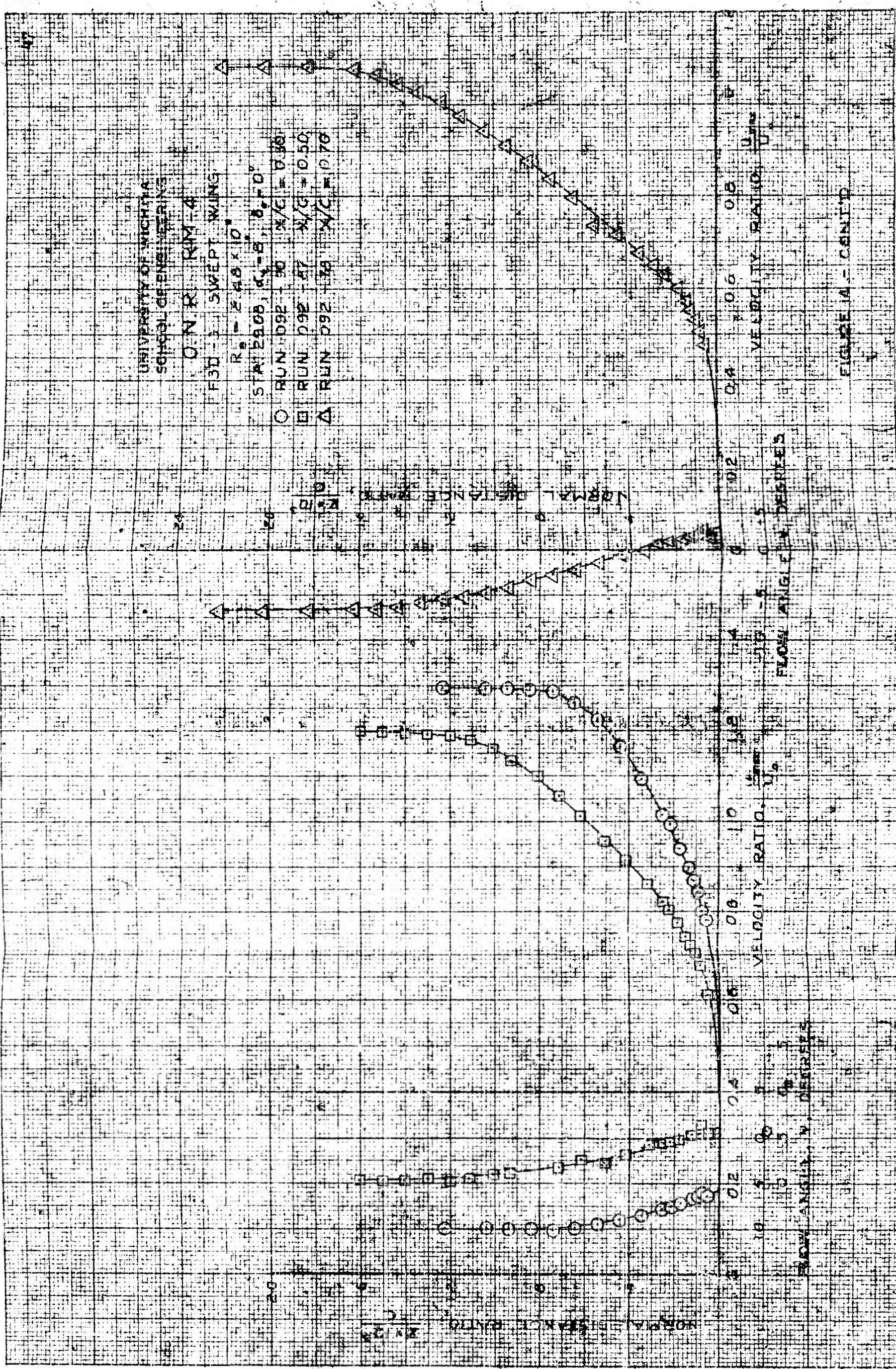
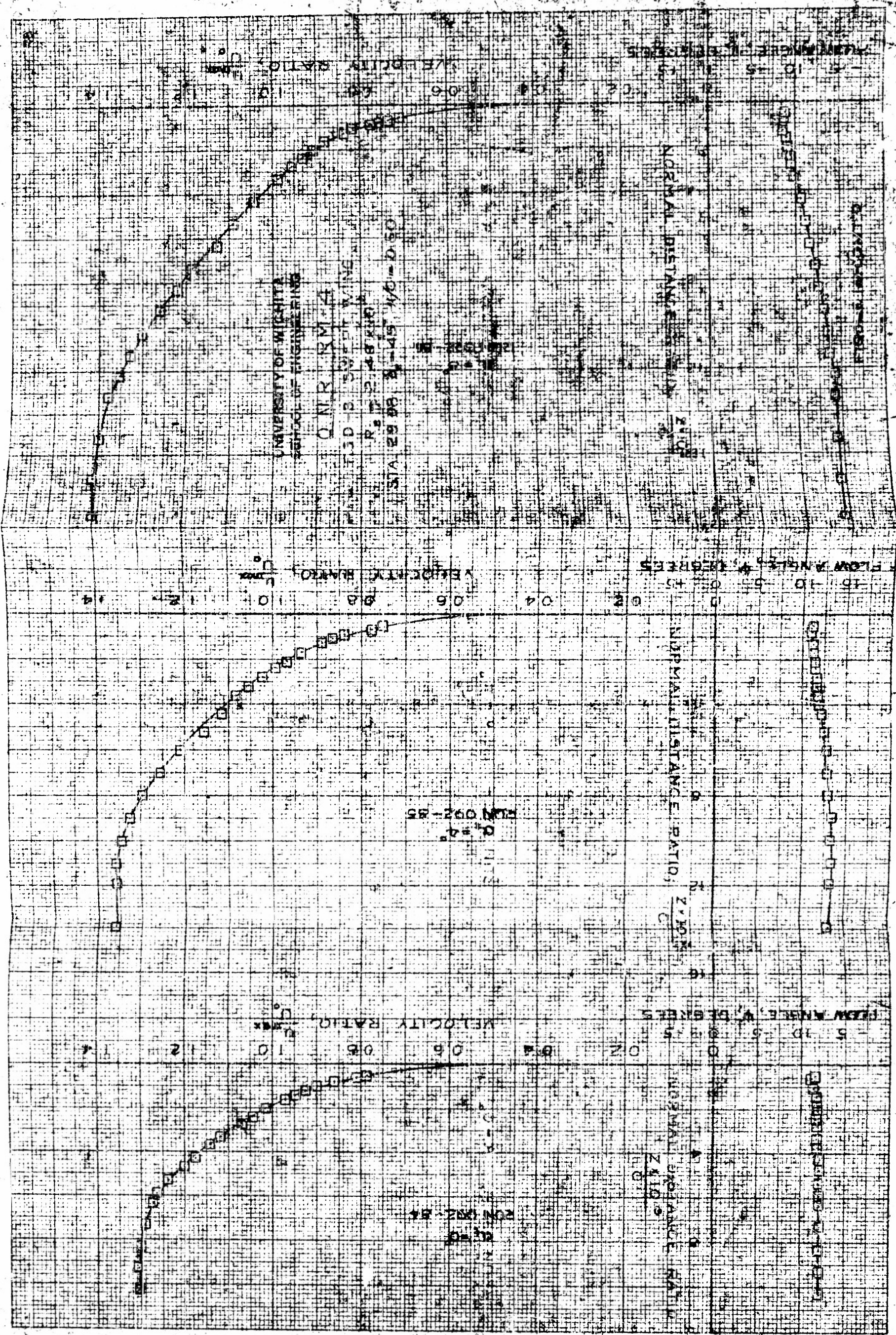


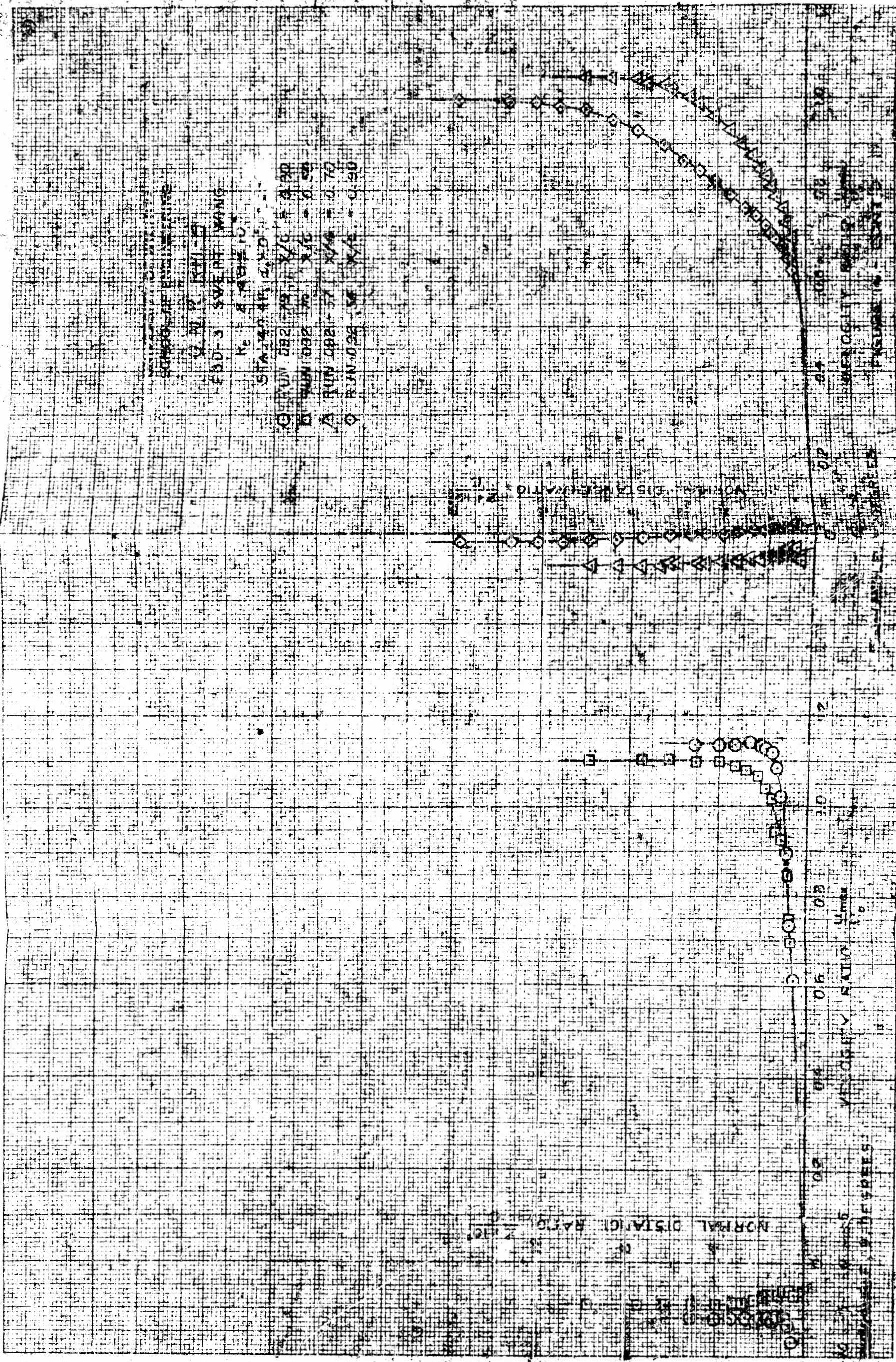
FIGURE E.1 - CRANE D

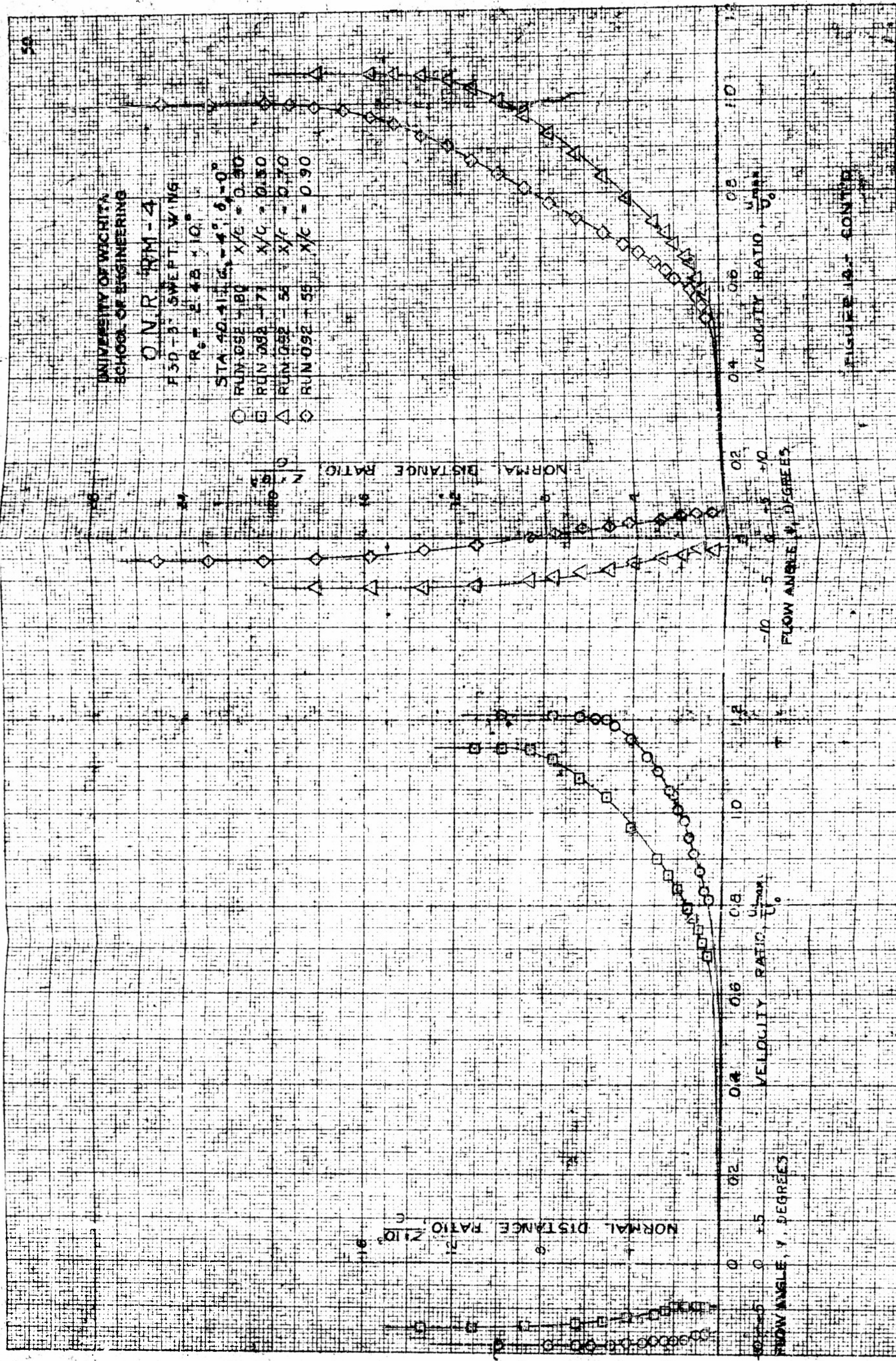


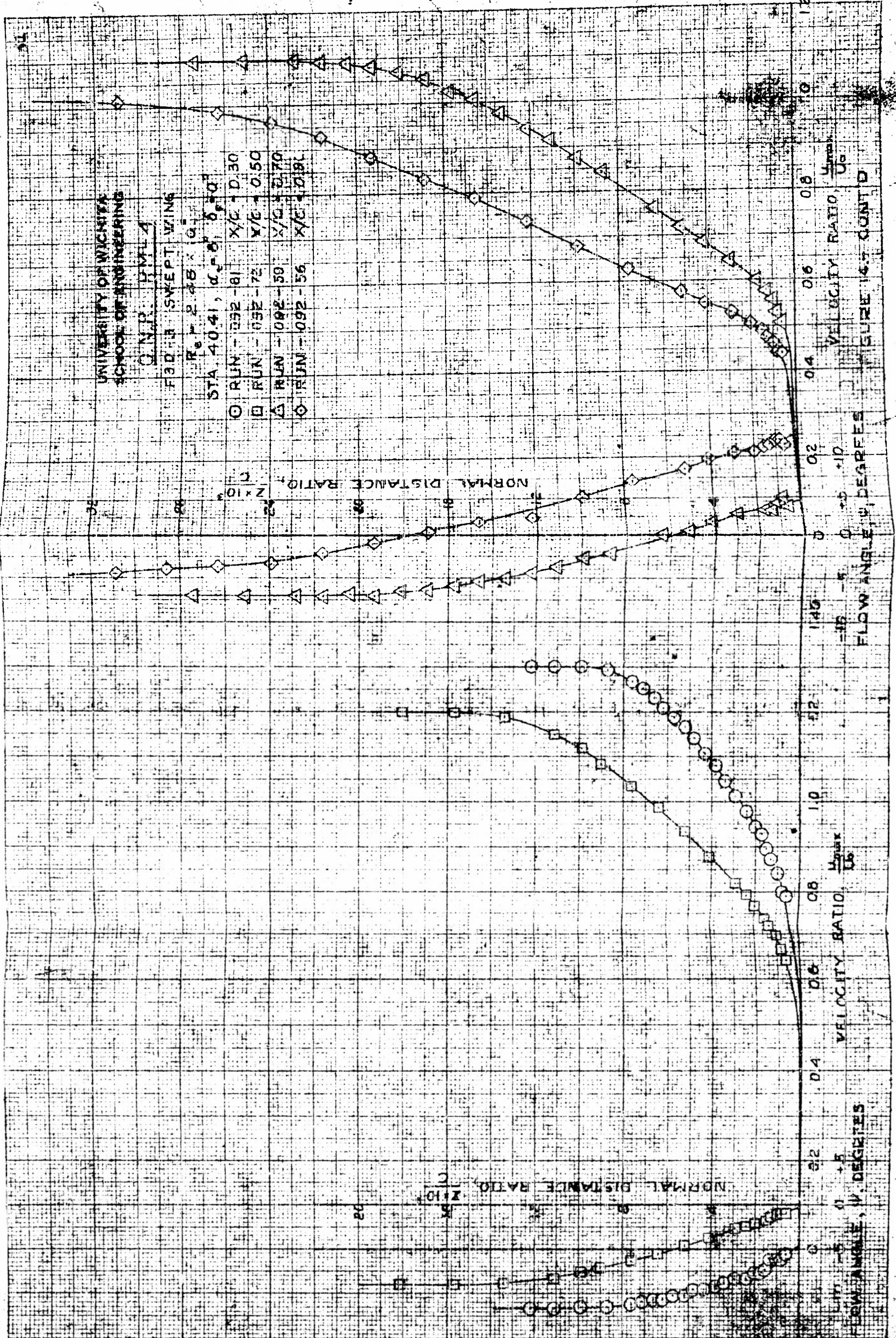












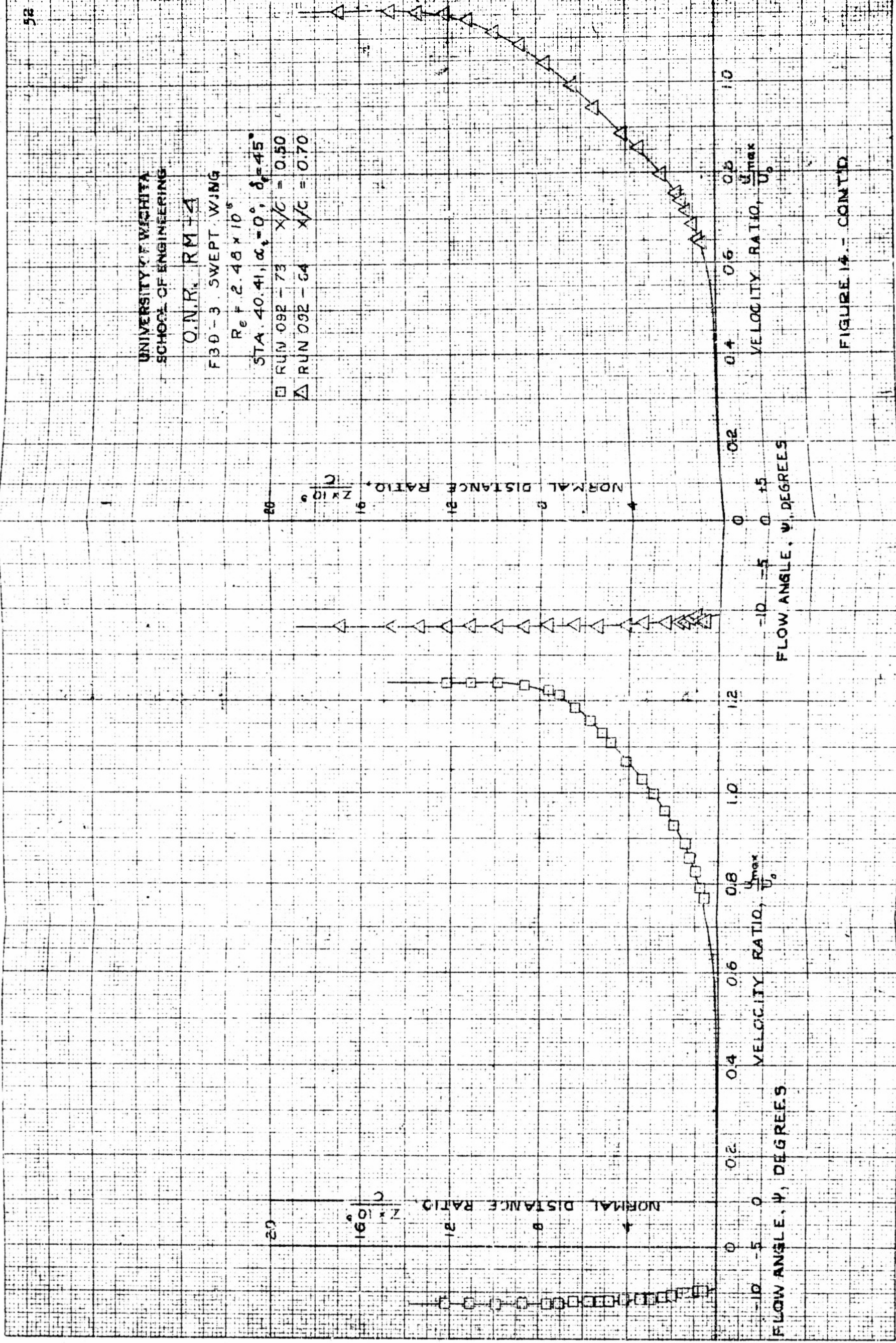


FIGURE 14.- CONT'D

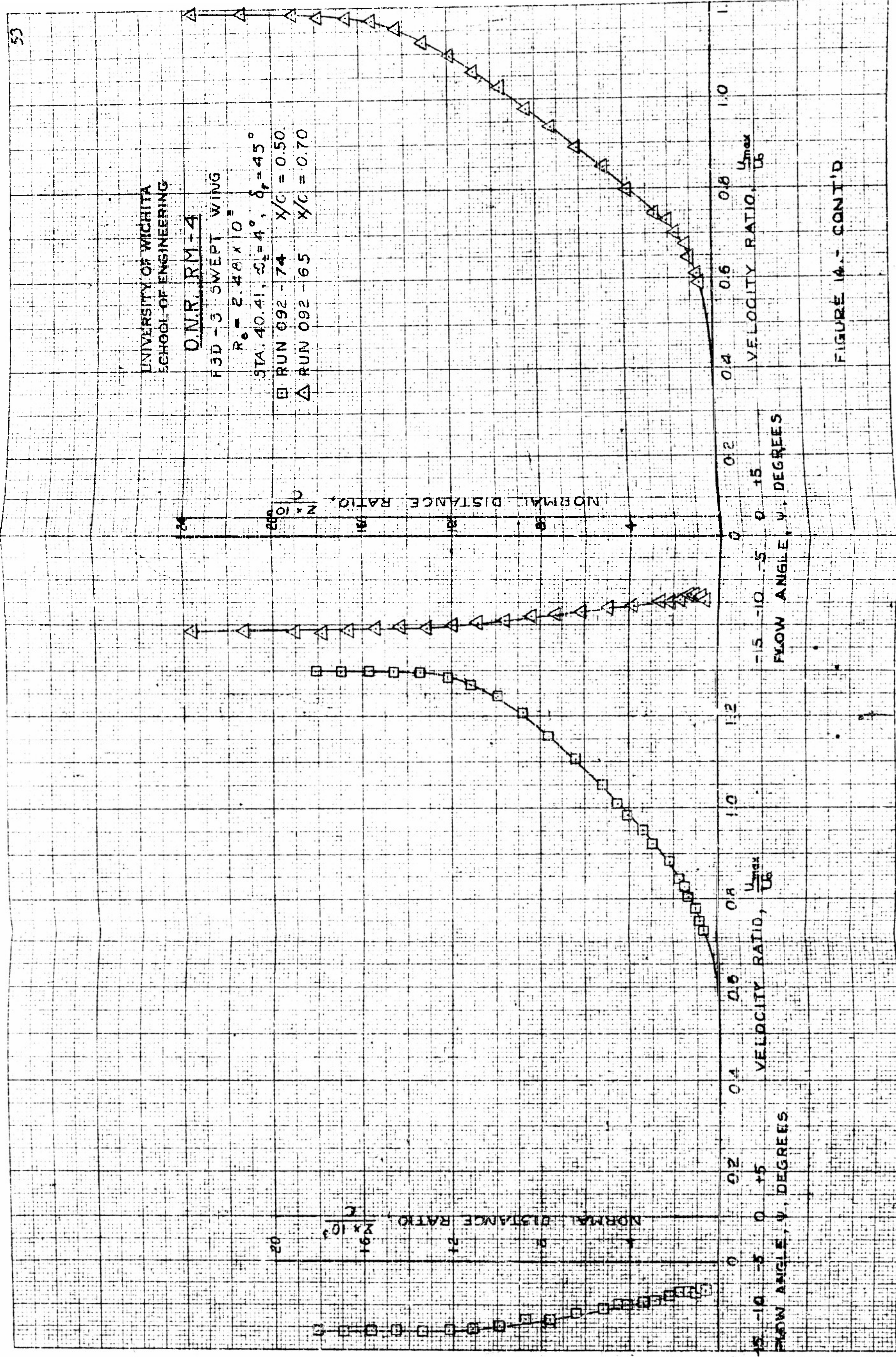


FIGURE 1a - CANT'D

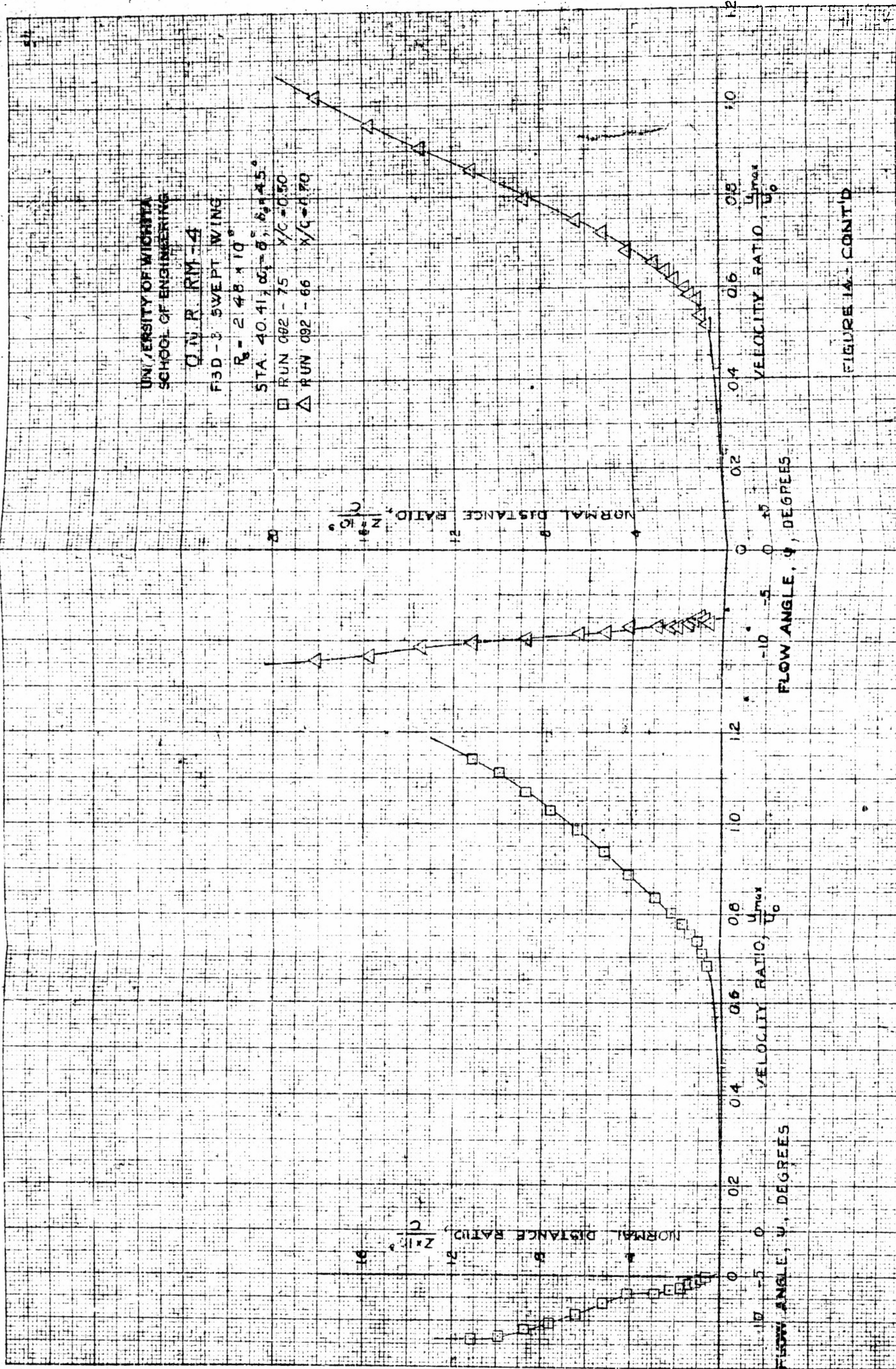


FIGURE 1A - CONT'D

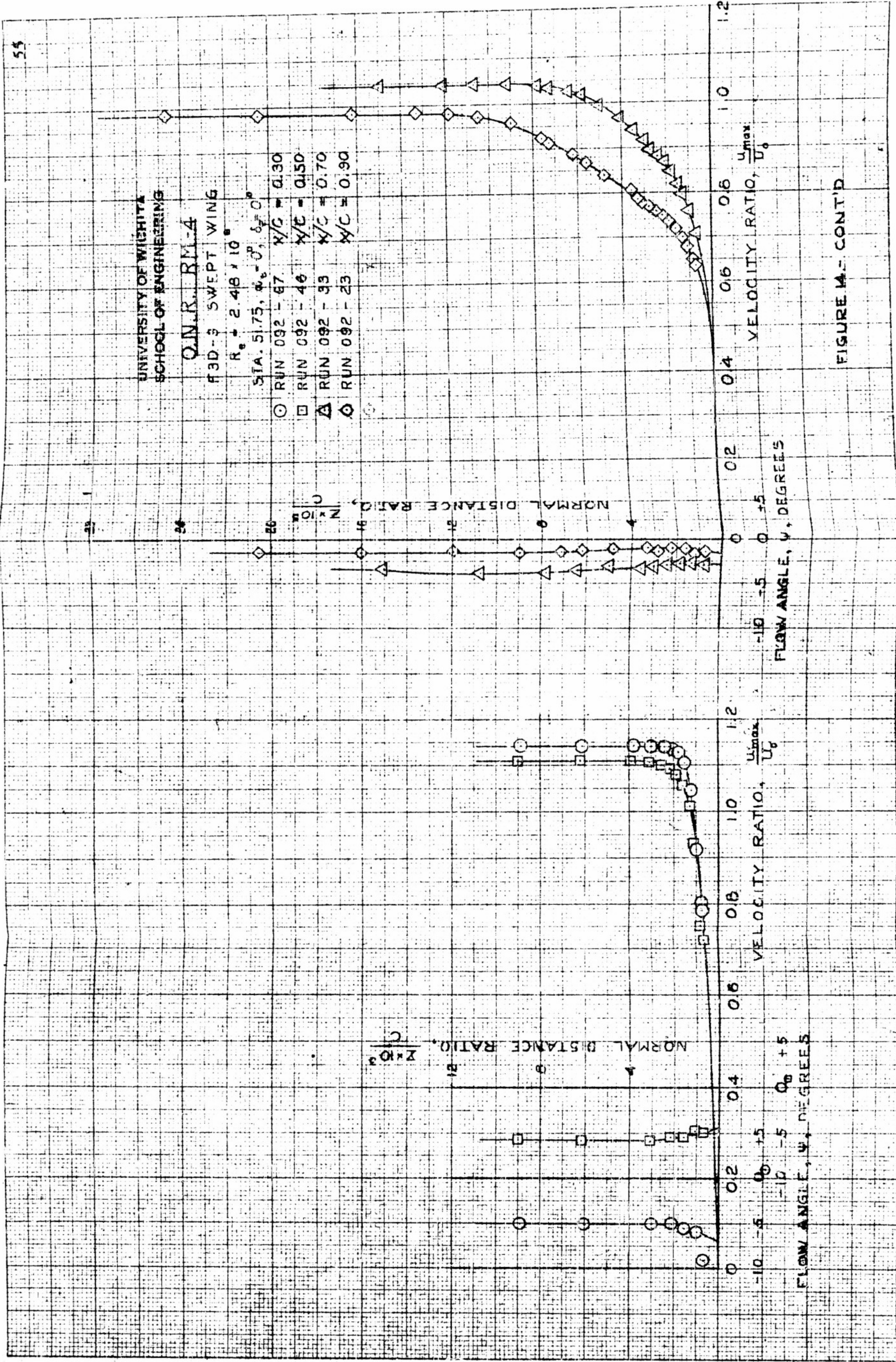


FIGURE IV—CONT'D

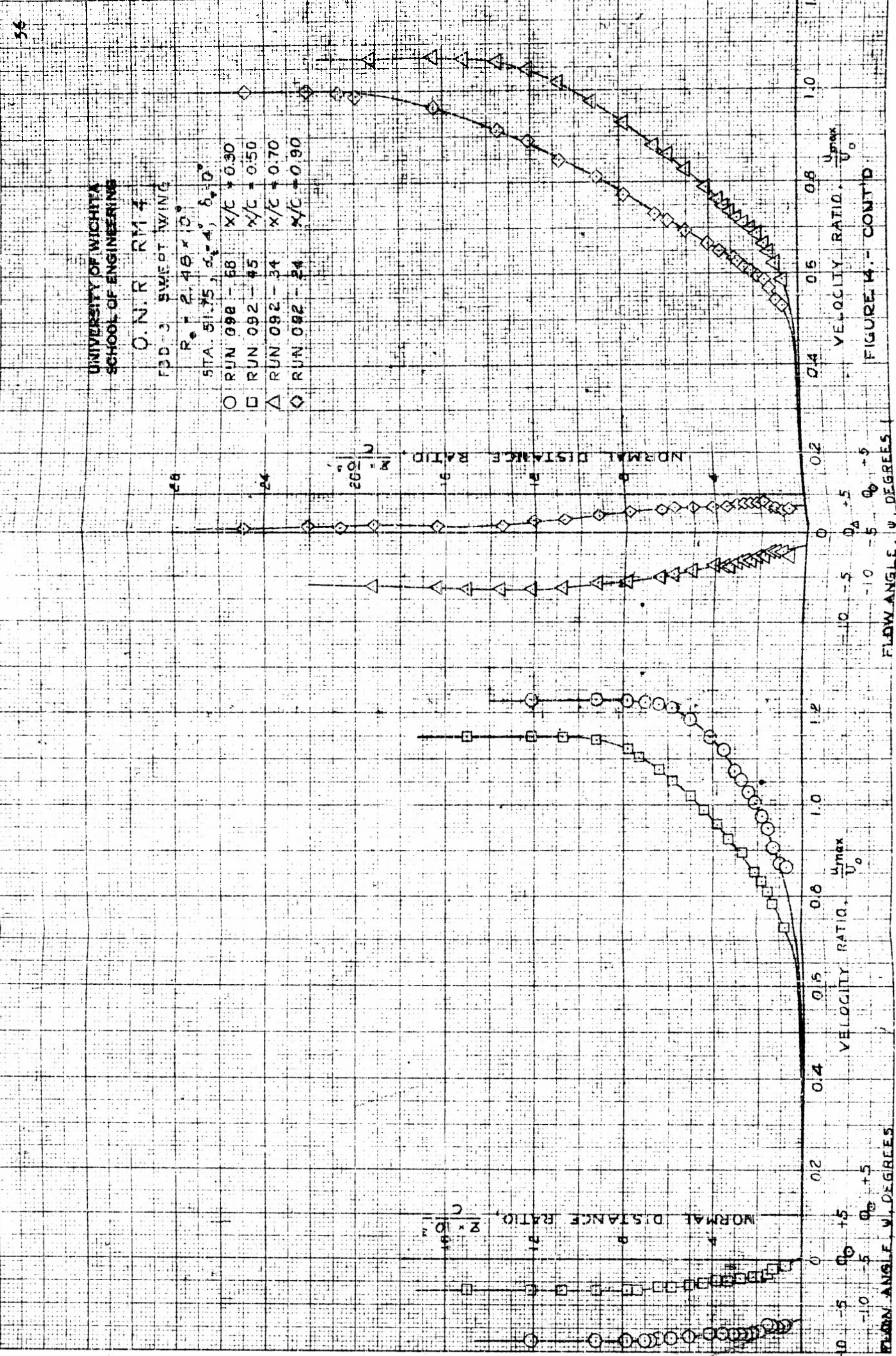


FIGURE 4.- CONT'D

Flow Angle, ψ , Degrees

Flow Angle, ψ , Degrees

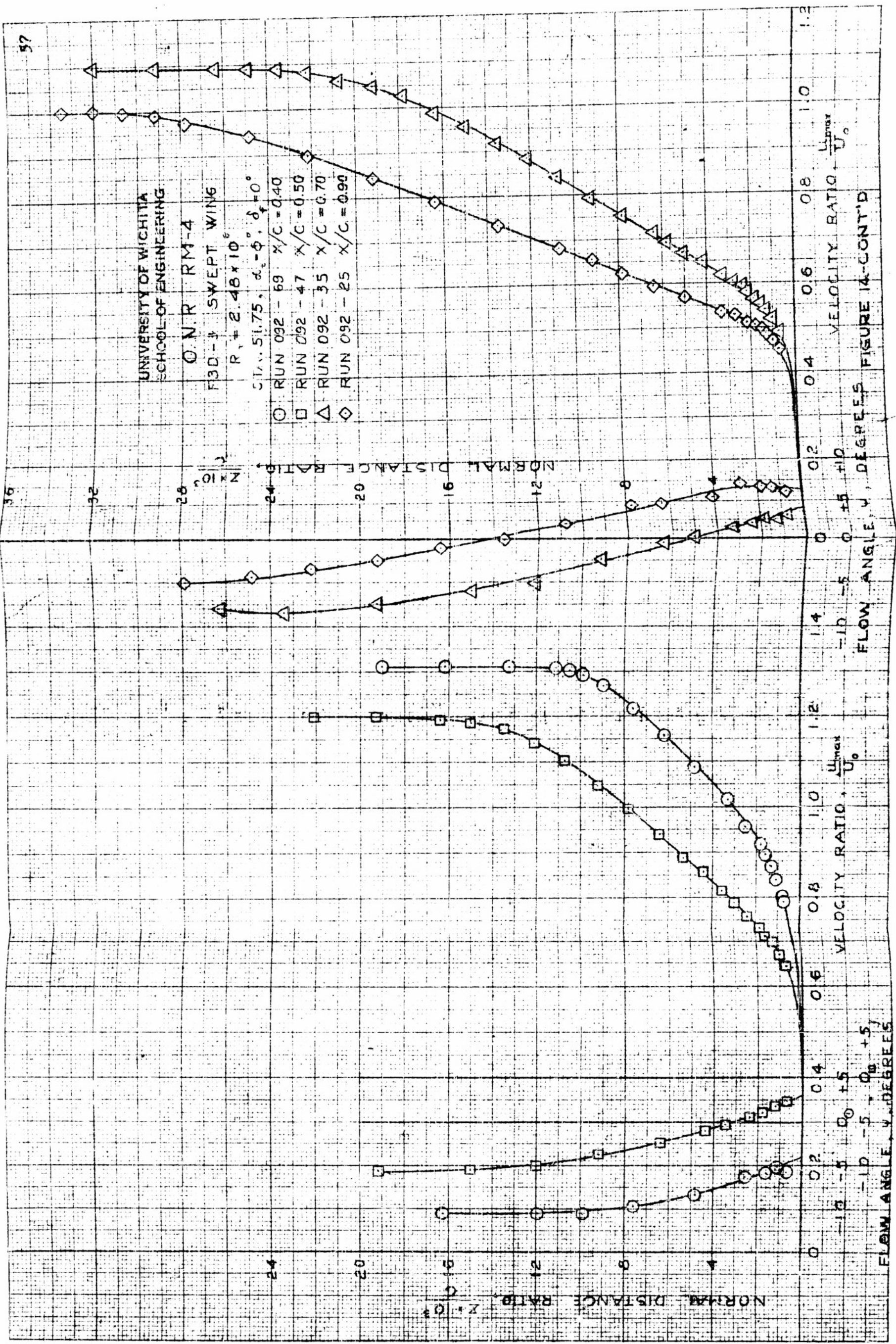
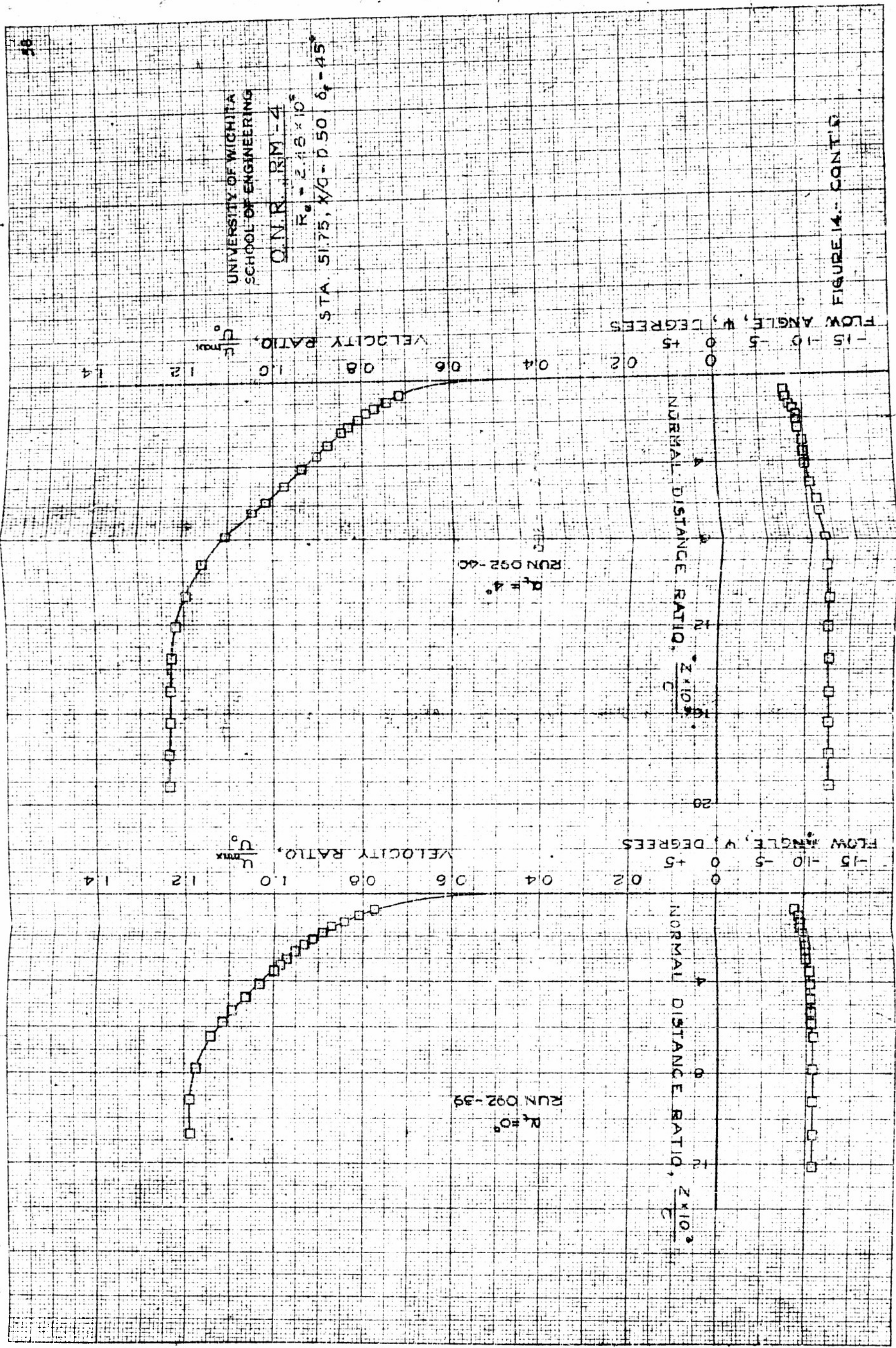


FIGURE 1A - CONT'D



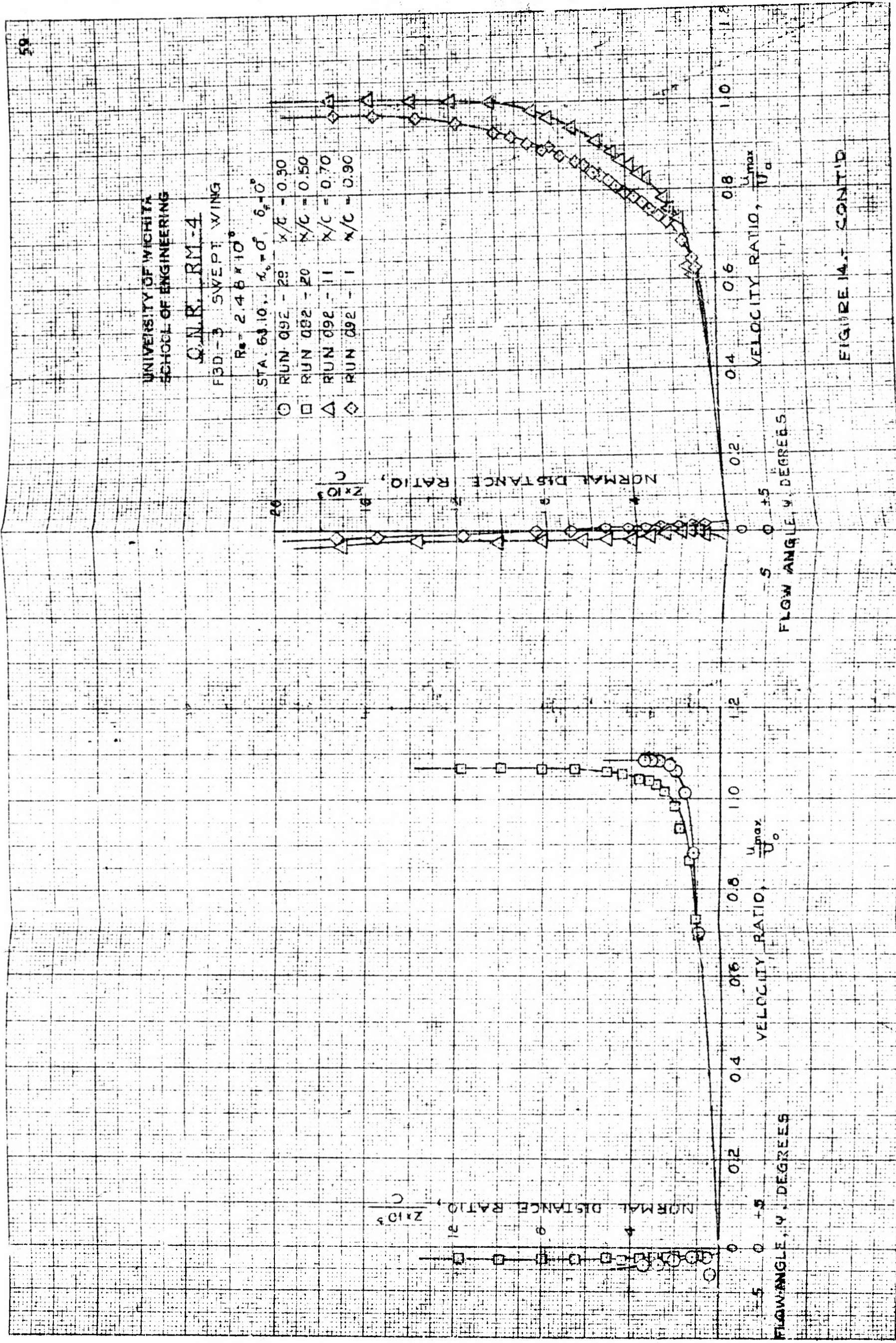
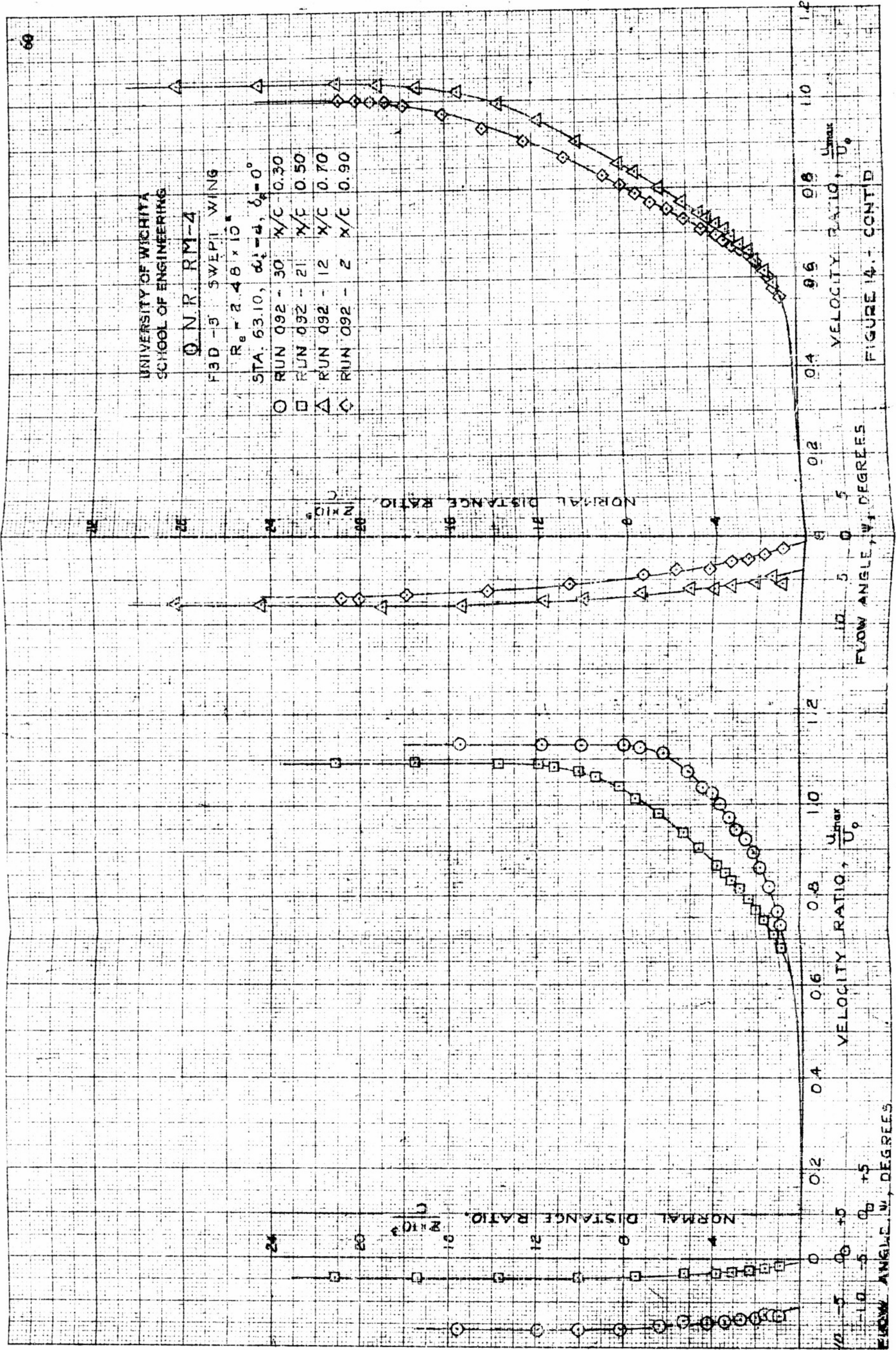
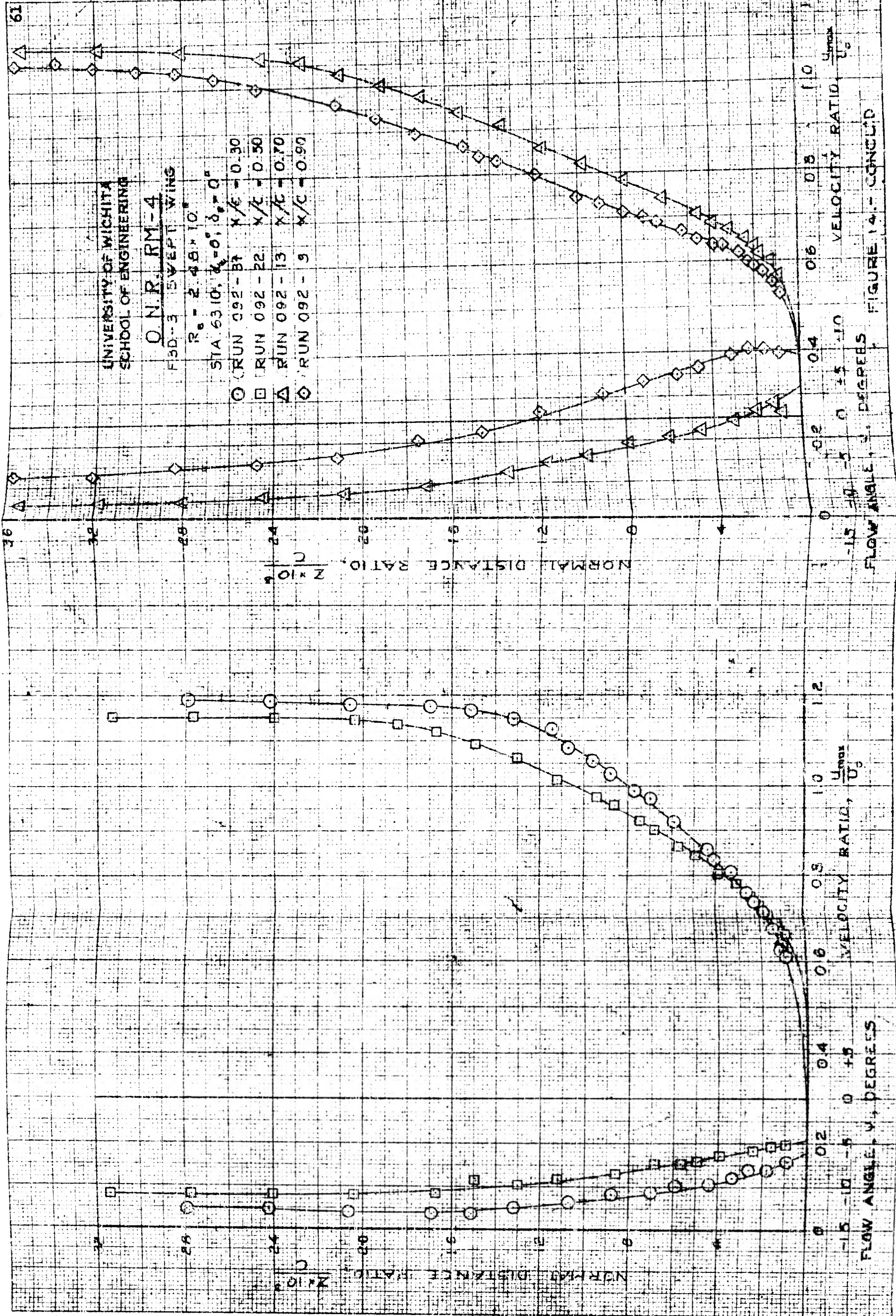


FIGURE 14.1 CONT'D





UNIVERSITY OF WICHITA
SCHOOL OF ENGINEERING

ENGR'D. DRAWING
SHAPE PARAPLATE, E.

SECTION
CHECK

1200

1000

800

600

400

200

0

LOCATED ON

SECTION OF PARAPLATE

SECTION PROJECTION

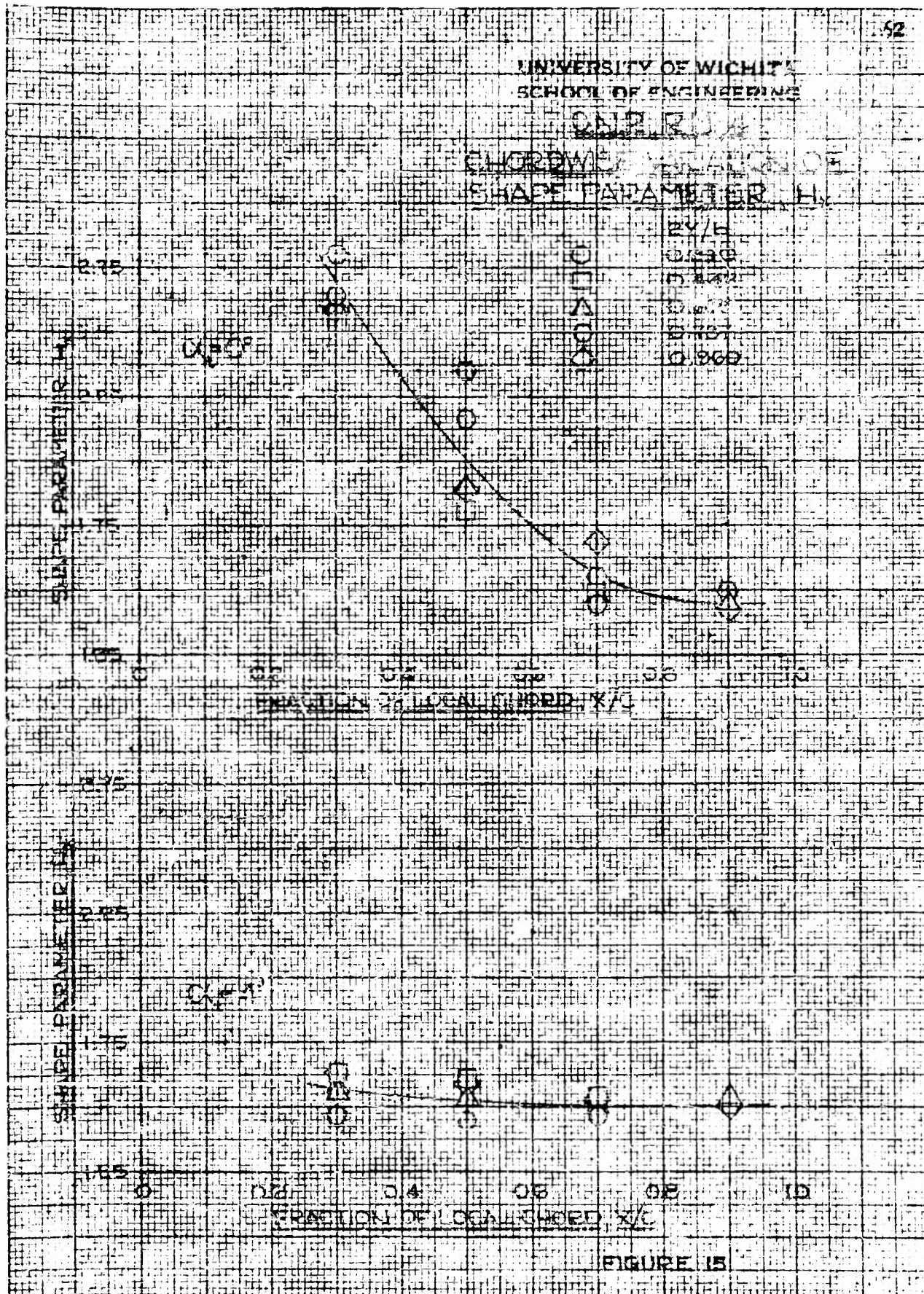
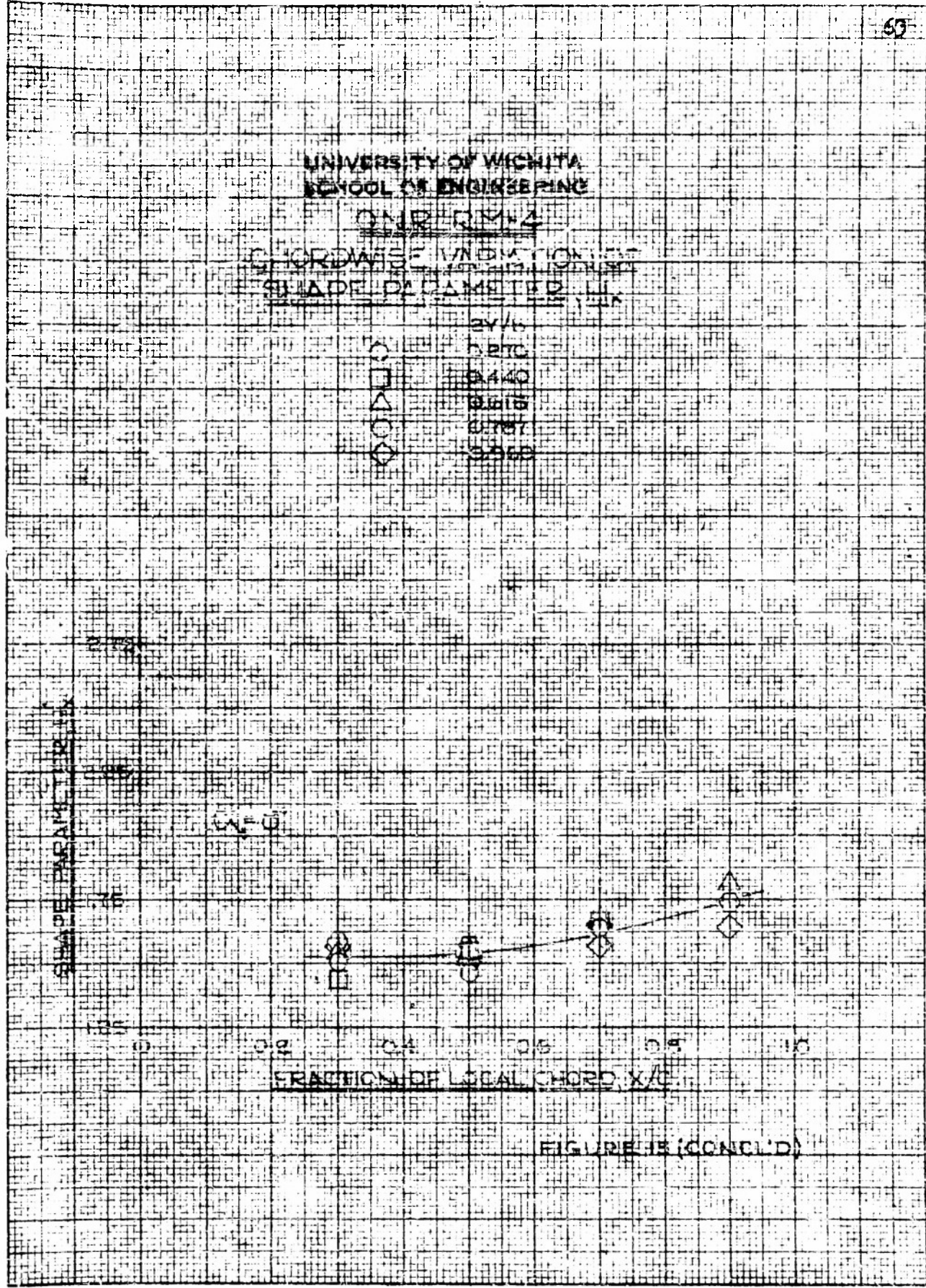
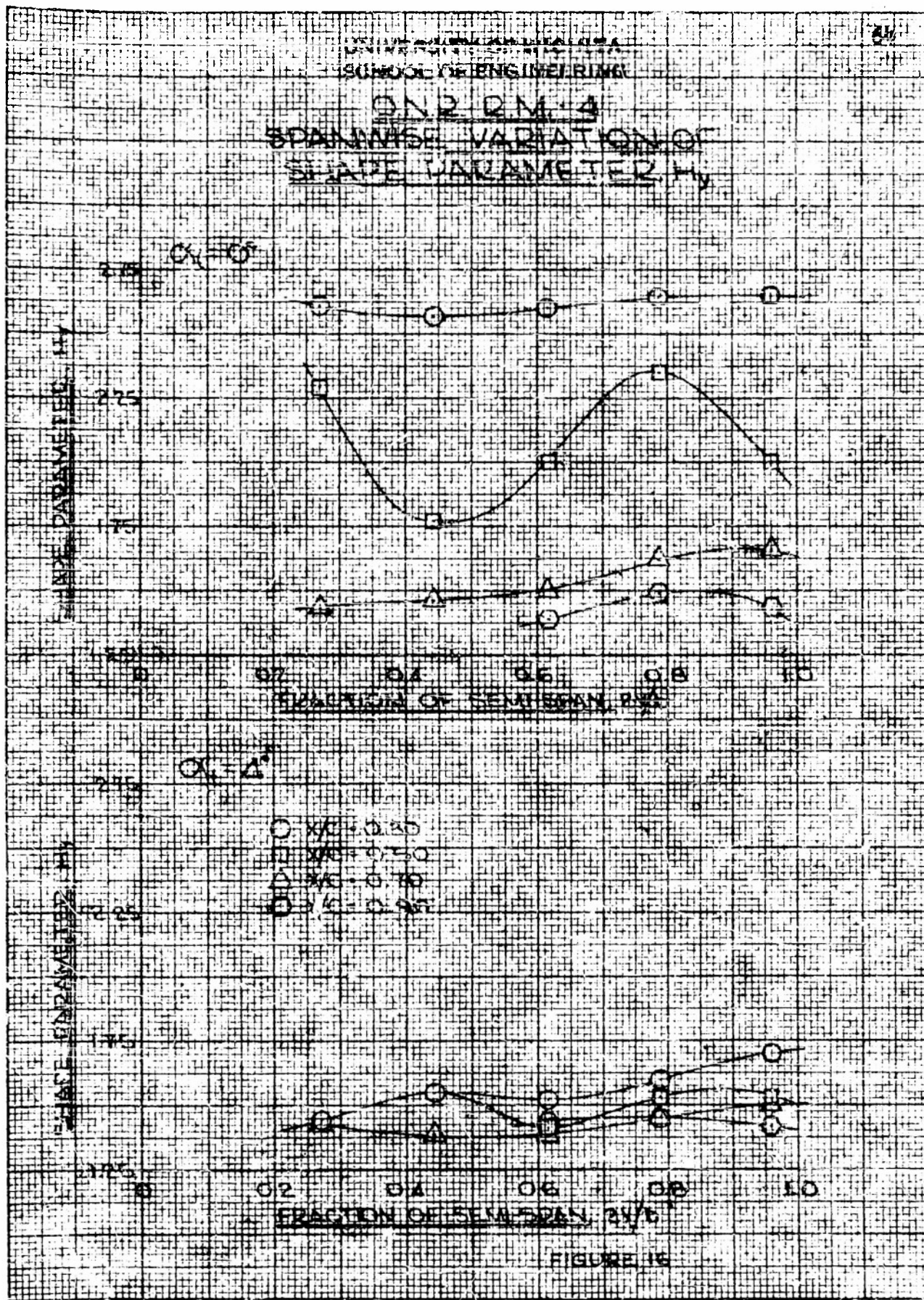


FIGURE 15





559-11 RECORDED BY FESSLER CO.
10-19-60 10:15 AM 1960

UNIVERSITY OF WICHITA
SCHOOL OF ENGINEERING

CLASS OF 1964

SPANWISE VIBRATION OF
PLATE DYNAMICS

CX B

O X O
O X O
O X O

FUNCTION OF SEMI SPAN TWO

FUNCTION OF SEMI SPAN ONE

Armed Services Technical Information Agency

Because of our limited supply, you are requested to return this copy WHEN IT HAS SERVED YOUR PURPOSE so that it may be made available to other requesters. Your cooperation will be appreciated.

AD

44732

NOTICE: WHEN GOVERNMENT OR OTHER DRAWINGS, SPECIFICATIONS OR OTHER DATA ARE USED FOR ANY PURPOSE OTHER THAN IN CONNECTION WITH A DEFINITELY RELATED GOVERNMENT PROCUREMENT OPERATION, THE U. S. GOVERNMENT THEREBY INCURS NO RESPONSIBILITY, NOR ANY OBLIGATION WHATSOEVER; AND THE FACT THAT THE GOVERNMENT MAY HAVE FORMULATED, FURNISHED, OR IN ANY WAY SUPPLIED THE SAID DRAWINGS, SPECIFICATIONS, OR OTHER DATA IS NOT TO BE REGARDED BY IMPLICATION OR OTHERWISE AS IN ANY MANNER LICENSING THE HOLDER OR ANY OTHER PERSON OR CORPORATION, OR CONVEYING ANY RIGHTS OR PERMISSION TO MANUFACTURE, USE OR SELL ANY PATENTED INVENTION THAT MAY IN ANY WAY BE RELATED THERETO.

Reproduced by
DOCUMENT SERVICE CENTER
KNOTT BUILDING, DAYTON, 2, OHIO

UNCLASSIFIED